AFRL-SR-BL-TR-99-

0077

REPORT DOCUMENTATION PAGE

1. AGENCY USE ONLY *(Leave blank)*	2. REPORT DATE	3. REPORT TYPE AND DATES COVERED
		15 JUL 96 TO 14 OCT 98 Final

4. TITLE AND SUBTITLE
MATERIAL AND DEVICE PROCESSING IMPROVEMENTS IN III-V NITRIDES

5. FUNDING NUMBERS
61101E
D144/08

6. AUTHOR(S)
PROFESSOR ABERNATHY

7. PERFORMING ORGANIZATION NAME(S) AND ADDRESS(ES)
University of Florida
205 Grinter Hall
Gainesville, FL 32611-5500

8. PERFORMING ORGANIZATION REPORT NUMBER

9. SPONSORING/MONITORING AGENCY NAME(S) AND ADDRESS(ES)
AFOSR/NE
801 North Randolph Street Rm 732
Arlington, VA 22203-1977

10. SPONSORING/MONITORING AGENCY REPORT NUMBER
F49620-96-1-0364

11. SUPPLEMENTARY NOTES

12a. DISTRIBUTION AVAILABILITY STATEMENT
APPROVAL FOR PUBLIC RELEASED; DISTRIBUTION UNLIMITED

12b. DISTRIBUTION CODE

13. ABSTRACT *(Maximum 200 words)*

We have examined the wet etching of AlN and $In_xAl_{1-x}N$ in KOH solutions as a function of crystal quality, etch temperature and compostion. AlN samples prepared by reactive sputtering on Si substrates at -200°C were annealed at temperatures from 400 to 1100°C and as expected, the etch rate decreased with anneal temperature, indicating improved crystal quality. We found that InAlN on Si substrates had higher wet etch rates. Both AlN and InAlN samples had an increase in etch rate with etch temperature. the etch rate for the InAlN increased as the in composition increased from 0 to 36%, and then decreased to zero for InN. Finally the effect of doping concentration in InAlN samples of similar In concentration (-3%) was examined and much higher etch rates were observed for the heavily doped material at solution temperatures above 60°C.

14. SUBJECT TERMS			15. NUMBER OF PAGES
			16. PRICE CODE
17. SECURITY CLASSIFICATION OF REPORT	18. SECURITY CLASSIFICATION OF THIS PAGE	19. SECURITY CLASSIFICATION OF ABSTRACT	20. LIMITATION OF ABSTRACT
UNCLASSIFIED	UNCLASSIFIED	UNCLASSIFIED	UL

DEVICE PROCESSING IMPROVEMENTS IN III-NITRIDES

GRANT NO. F49620-96-1-0364

FINAL REPORT

C. R. Abernathy

Rhines Hall
Department of Materials Science and Engineering
University of Florida
Gainesville, FL 32611

PROGRAM ACCOMPLISHMENTS

Etching

Wet Etching

Only molten salts such as KOH or NaOH at temperatures above ~250°C have been found to etch GaN at practical rates, and the difficulty of handling these mixtures and the inability to find masks that will hold up to them has limited the application of wet etching in GaN device technology. We have found that AlN and Al-rich alloys can be wet etched in KOH at temperatures of 50-100°C.[1] A compilation of etch results for binary and ternary nitrides is shown in Table I. These results are for non light-assisted conditions. For single crystal AlN we find that KOH-based solutions, such as AZ400K developer, produce reaction-limited etching with an activation energy of ~15.5 kCal·mol^{-1} (Figure 1). The rates are a strong function of material quality, with higher quality AlN etching at a slower rate.

We have examined the wet etching of AlN and $In_XAl_{1-X}N$ in KOH solutions as a function of crystal quality, etch temperature and composition. AlN samples prepared by reactive sputtering on Si substrates at ~200°C were annealed at temperatures from 400 to 1100°C and as expected, the etch rate decreased with anneal temperature, indicating improved crystal quality. We found that InAlN on Si substrates had higher wet etch rates. Both AlN and InAlN samples had an increase in etch rate with etch temperature. The etch rate for the InAlN increased as the In composition increased from 0 to 36%, and then decreased to zero for InN. Finally the effect of doping concentration in InAlN samples of similar In concentration (~3%) was examined and much higher etch rates were observed for the heavily doped material at solution temperatures above 60°C.

The AlN was reactively sputter deposited on a Si substrate to a thickness of ~1200Å using a N_2 discharge and a pure Al target. This type of AlN film has been shown to be an effective annealing cap for GaN at a temperature of 1100°C. The InAlN samples were grown using metalorganic molecular beam epitaxy (MOMBE) on semi-insulating, (100) GaAs substrates or *p*-type (1Ωcm) Si substrates in an Intevac Gen II system.[2] The group III sources were triethylgallium, dimethylethylamine alane and trimethylindium, respectively, and the atomic nitrogen was derived from an ECR Wavemat source operating at 200 W forward power. The layers were single crystal with a high density (10^{11} to 10^{12}cm^{-2}) of stacking faults and microtwins. InAlN samples were found to contain both hexagonal and cubic forms. The $In_XAl_{1-X}N$ layers were either conducting *n*-type as grown (~10^{18}cm^{-3}) for $x \geq 0.03$ due to residual autodoping by native defects or fully depleted for $x < 0.03$. The compositions examined were 100, 75, 36, 29, 19, 3.1, 2.6 and 0% In.

Table I. Compilation of etching results in acid and base solutions, performed at room temperature (25°C) unless otherwise noted.

	GaN	InN	AlN	InAlN	InGaN
Citric Acid (75°C)	0	0	0	0	0
Succinic acid (75°C	0	0	0	0	0
Oxalic acid (75°C)	0	Lifts off	Lifts off	Lifts off	Lifts off
Nitric acid (75°C)	0	Lifts off	Lifts off	Lifts off	Lifts off
Phosphoric acid (75°C)	0	0	Oxide removed	Oxide removed	0
Hydrochloric acid (75°C)	0	0	0	0	0
Hydrofluoric acid	0	Lifts off	0	0	Lifts off
Hydriodic acid	0	0	0	0	0
Sulfuric acid (75°C)	0	Lifts off	0	0	0
Hydrogen peroxide	0	0	0	0	0
Potassium iodide	0	0	0	0	0
2% Bromine-methanol	0	0	0	0	0
n-Methyl-2-pyrrolidone	0	0	0	0	0
Sodium hydroxide	0	Lifts off	Lifts off	Lifts off	Lifts off
Potassium hydroxide	0	Lifts off	22,650 Åmin^{-1}	0	0
AZ400K Photoresist developer (75°C)	0	Lifts off	~60-10,000 Åmin^{-1}	Composition dependent	0
Hydriodic acid/hydrogen peroxide	0	0	0	0	0
Hydrochloric acid/hydrogen peroxide	0	0	0	0	0
Potassium triphosphate (75°C)	0	0	0	0	0
Nitric acid/potassium triphosphate (75°C)	0	Lifts off	0	0	0
Hydrochloric acid/potassium triphosphate (75°C)	0	0	0	0	0
Boric acid (75°C)	0	0	0	0	0
Nitric/boric acid (75°C)	0	Lifts off	0	0	Lifts off
Nitric/boric/hydrogen peroxide	0	Lifts off	0	0	Removes oxide
$HCl/H_2O_2/HNO_3$	0	Lifts off	0	Lifts off	Lifts off
Potassium tetraborate (75-°C)	0	Oxide removal	Oxide removal	Oxide removal	Oxide removal
Sodium tetraborate (75°C)	0	0	0	0	0
Sodium tetraborate/hydrogen peroxide	0	0	0	0	0
Potassium triphosphate (75°C)	0	0	0	0	0
Potassium triphosphate/hydrogen peroxide	0	0	0	0	0

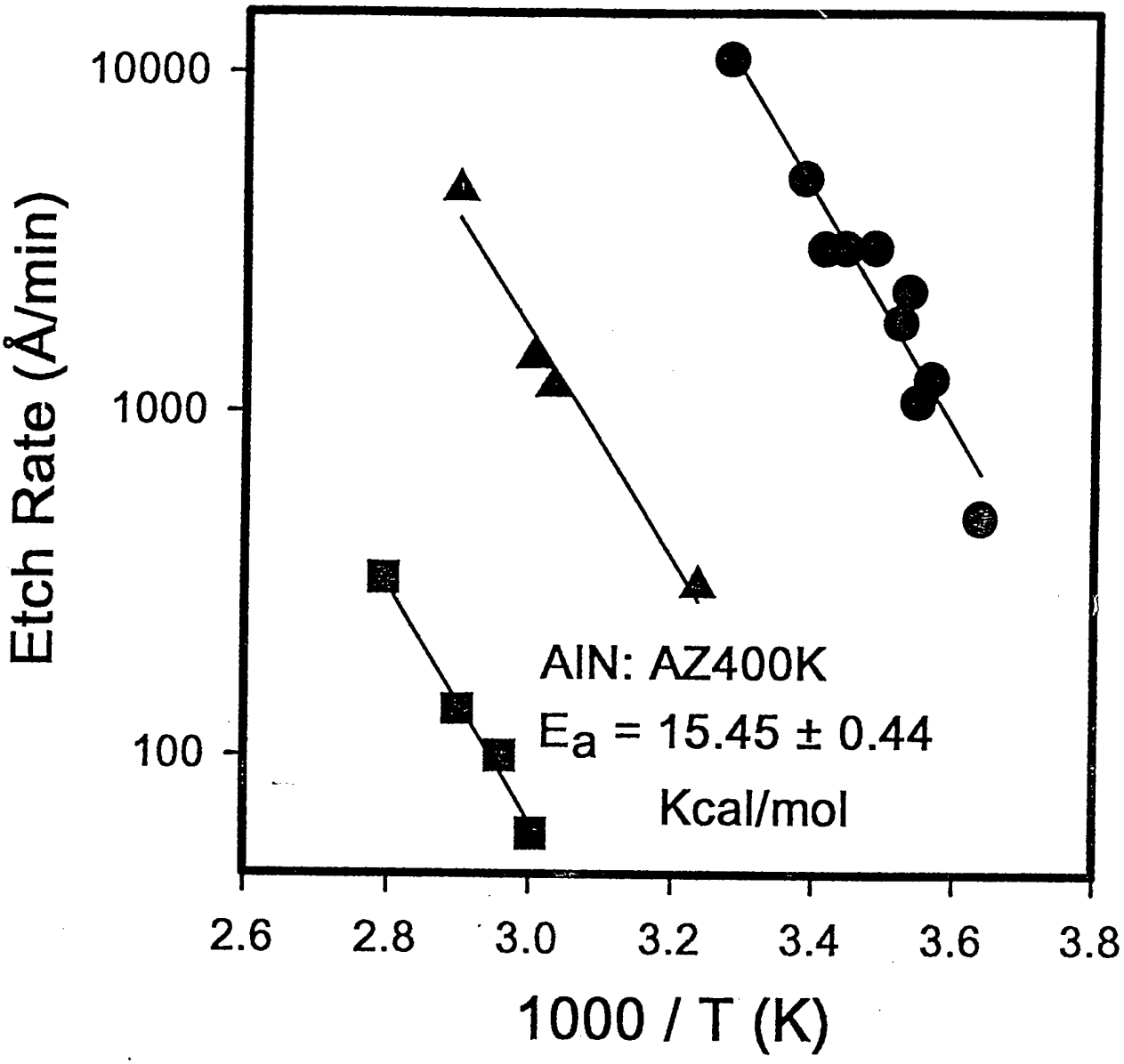

Figure 1. Arrhenius plot of etch rate of three different AlN samples in AZ400K developer solution. The higher the AlN quality, as measured by XRD, the slower the etch rate.

The AlN samples were annealed in a RTA system (AG410T) face down on a GaAs substrate for 10 sec at temperatures between 500 and 1150°C in a N_2 atmosphere. For wet etching studies, all samples were masked with Apiezon wax patterns. Etch depths were obtained by Dektak stylus profilometry after the removal of the mask with an approximate 5% error. Scanning electron microscopy (SEM) was used to examine the undercutting on the etched samples. AZ400K developer solution, with an active ingredient KOH[3], was used for the etch, and etch temperatures between 20 and 80°C.

Figure 2 shows the etch rate of the sputtered AlN as a function of etch temperature for samples as grown or annealed at 500, 700, 900, 1000 and 1100°C. The etch rates of both the as-deposited and 500°C annealed sample increase sharply as the etch temperature increases from 20 to 50°C, and then level off; the rate drops by approximately 10% with a 500°C anneal. The samples annealed at 700, 900 and 1000°C also show similar trends, with a monotomic decrease in rate for higher anneal temperatures. The crystal quality appears to increase significantly with anneal temperature as the etch rate drops accordingly. The etch rate continues to drop by ~10% with each successive anneal, to 1000°C. After 1100°C the etch rate drops and is less temperature dependent. Overall there is an ~90% reduction in etch rate from the as-deposited AlN to that annealed at 1100°C for etching at 80°C.

The activation energy for an etch solution can be determined from an Arrhenius plot, and is shown in Figure 3. The activation energies for all samples was the same within experimental error, 2.0 ± 0.5 kcal mol^{-1}. This is indicative of a diffusion-limited reaction. This is much lower than the activation energy of 15.45 kcal mol^{-1} reported by Mileham et.al.[3] for AlN grown by metalorganic molecular beam epitaxy. The quality of the material in the current experiment is much lower though, and the etch may be proceeding at such a rapid rate that the solution is becoming depleted of reactants near the materials surface.

The etch rate as a function of solution temperature for $In_xAl_{1-x}N$ grown on either GaAs or Si, for 19% In is shown in Figure 4. At 20°C etch temperature there is no difference in etch rate. The etch rates for both materials increase with etch temperature, with the differential in etch rates also increasing with temperature. As was mentioned previously, the InAlN grown on Si has a greater concentration of crystalline defects as evident from x-ray diffraction and absorption measurements. At 80°C the etch rate for the film on the Si substrate is approximately three times faster than for the film grown on GaAs. This is another clear indication of the dependence of wet etch rate on material quality and emphasizes why it has proven very difficult to find etch solutions for high quality single-crystal nitrides.

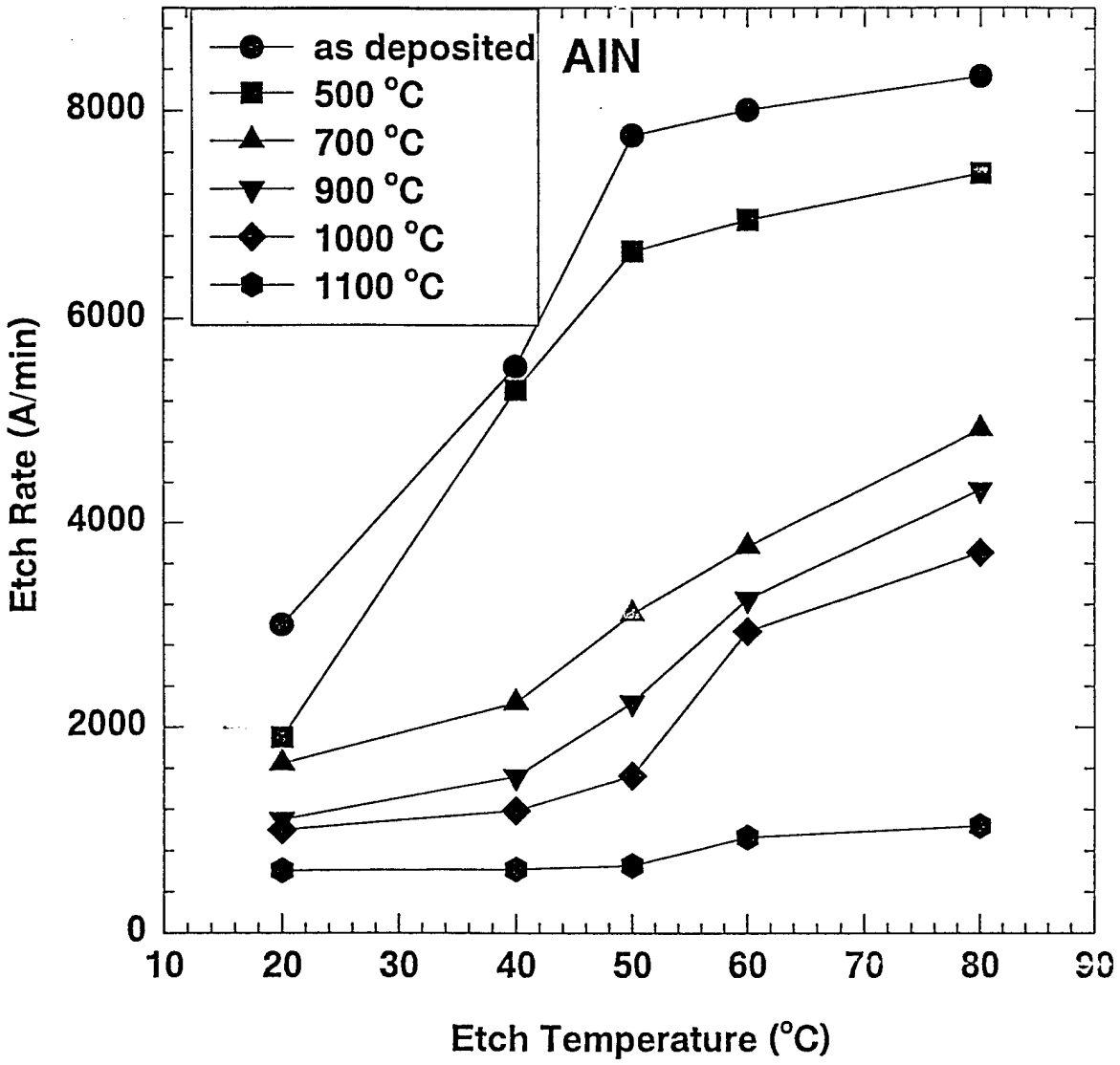

Figure 2. Etch rate of AlN as a function of etch temperature for samples as-deposited or annealed at 500, 700, 900, 1000 and 1100°C.

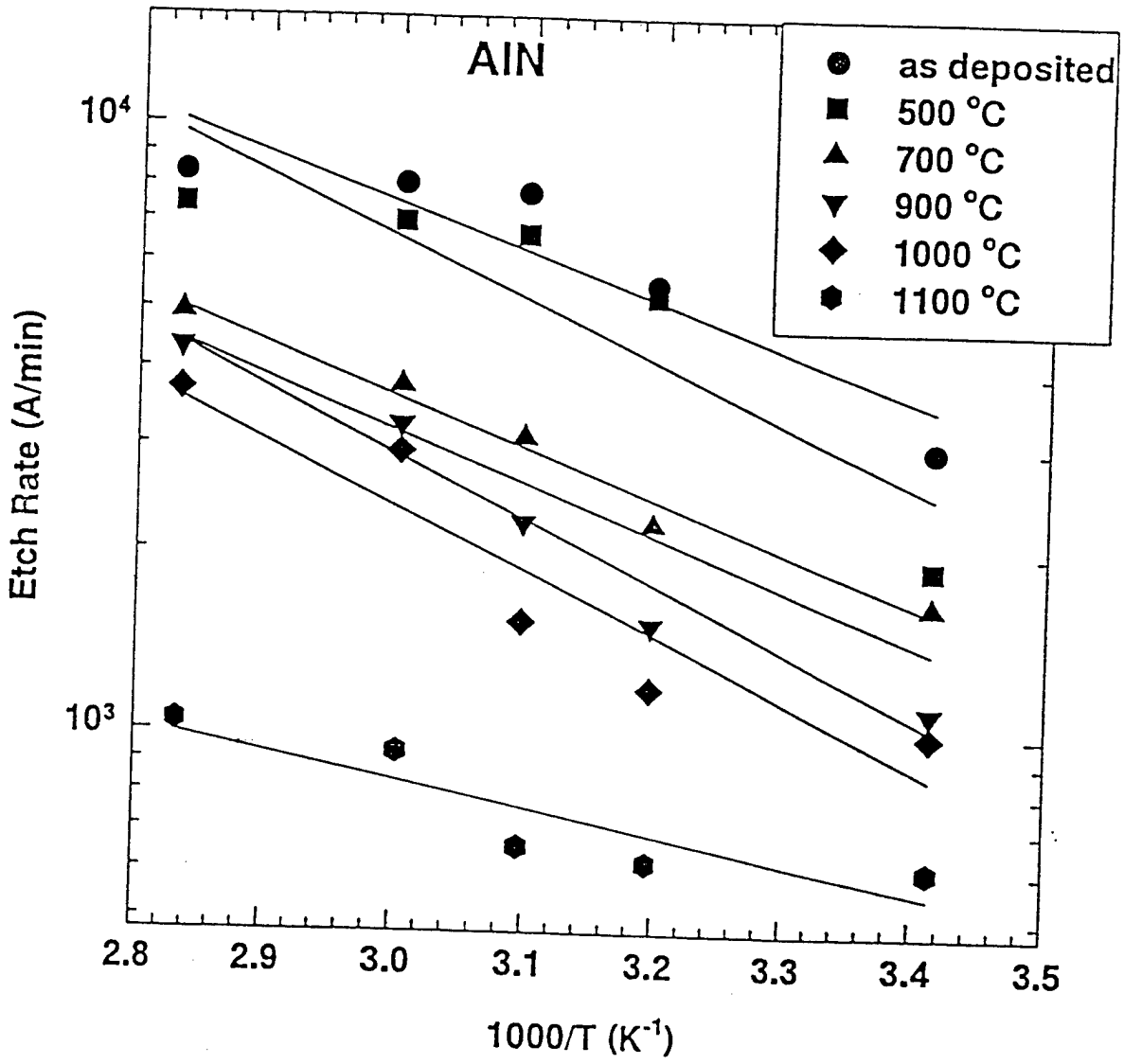

Figure 3. Arrhenius plots of etch rates for as-deposited or annealed AlN as a function of reciprocal etch temperature.

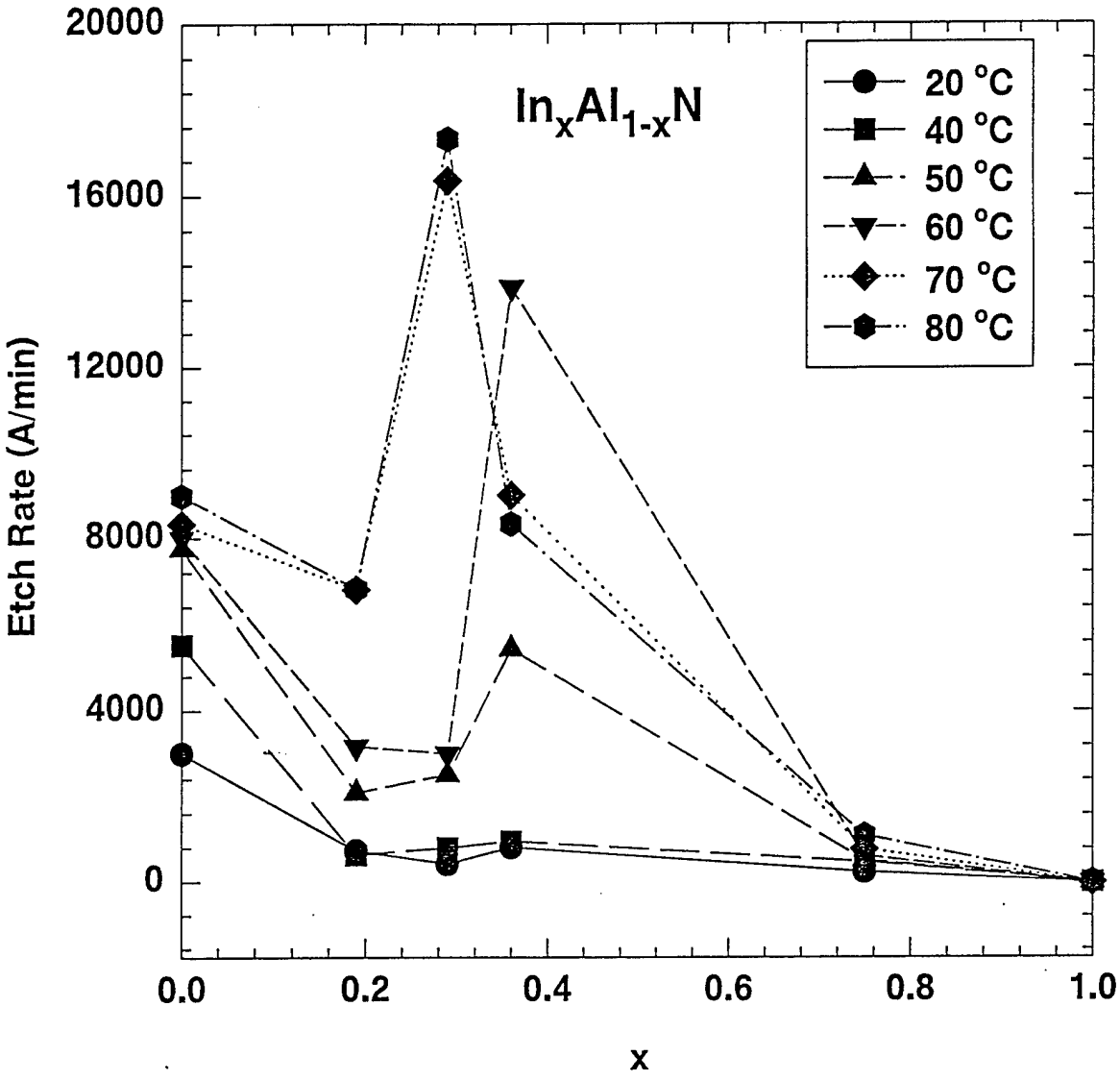

Figure 4. Etch rates as a function of etch temperature for $In_XAl_{1-X}N$ grown on GaAs and Si for 19% In.

Etch rates for $In_xAl_{1-X}N$ grown on GaAs for $0 \leq x \leq 1$ are shown in Figure 5, for etch temperatures between 20 and 80°C. Up to 40°C the etch rates are very low and show little dependence on In composition. The AlN etches much faster at these temperatures than any composition of the ternary alloy InAlN. As the etch temperature increases to 60°C, the etch rates increase, showing a peak for 36% In. This is presumably due to a tradeoff between the reduction in average bond strength for InAlN relative to the pure binary AlN, and the fact that the chemical sensitivity falls off at higher In concentrations. Thus the etch rates initially increase for increasing In, but then decrease at higher concentrations because there is no chemical driving force for etching to occur. InN did not etch in this solution at any temperature but was occasionally lifted off during long etches because of the defective interfacial region between InN and GaAs being attached by the KOH.

Arrhenius plots of etch rates for $In_xAl_{1-X}N$ for $0 \leq x \leq 1$ giving activation energies for the etches are shown in Figure 6. There is substantial scatter in the data, but the activation energies are all in the range 2-6 kcal mol^{-1}, which again is consistent with diffusion-controlled etching. This is not desirable for device fabrication processes because the rates are then dependent on solution agitation and the etched surface morphology are generally rougher than for reaction-controlled solutions.

Apart from material quality or composition, another factor which often plays a role in determining etch rates is sample conductivity. Figure 7 shows a plot of InAlN etch *vs.* etch rate temperature for samples with 2.6 and 3.1% In, which were depleted ($n < 10^{16} cm^{-3}$) and doped at $n \sim 5x10^{18} cm^{-3}$, respectively. Since the autodoping changes rapidly around this composition, but there is little change in In concentration, these samples represent a good test of any effects related to conductivity. The samples have similar etch rates at low solution temperatures. Above 60°C, however, the *n*-type sample etch rate increases more rapidly, approximately two times faster than the depleted sample. These results indicate that at temperatures where fast etch rates occur, the electrons in the *n*-type sample are part of the chemical reaction between the OH^- ions and the Al in the InAlN film. They may enhance formation of these ions initially and thus the etch rate is enhanced. It will be interesting to try *p*-type InAlN.

Etching with KOH-based solution is completely selective for InAlN over GaN or InN. Annealing of sputtered AlN improved the crystal quality of the film, decreasing the chemical etch rate in KOH-based solutions. InAlN etch rates also increased with decreasing crystalline quality. Both AlN and InAlN samples had activation energies for etching in KOH $\leq$6 kcal mol^{-1}, etch which is typical of a diffusion-controlled etch mechanism. The etch rate for the InAlN initially increased as the In composition increased from 0 to 36%, and then decreased to zero for pure InN. The *n*-type InAlN etched approximately two times faster than the undoped material above 60°C, indicating that electrons play a role in the etch mechanism.

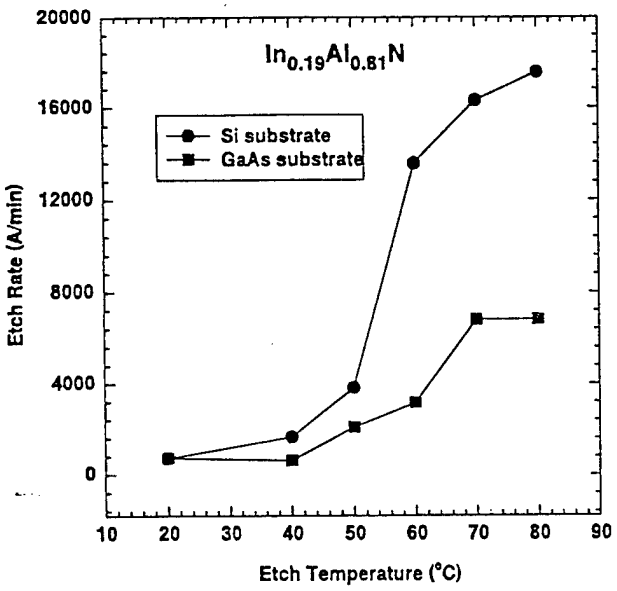

Figure 5. Etch rate for $In_XAl_{1-X}N$ for $0 \leq x \leq 1$ at solution temperatures between 20 and 80°C.

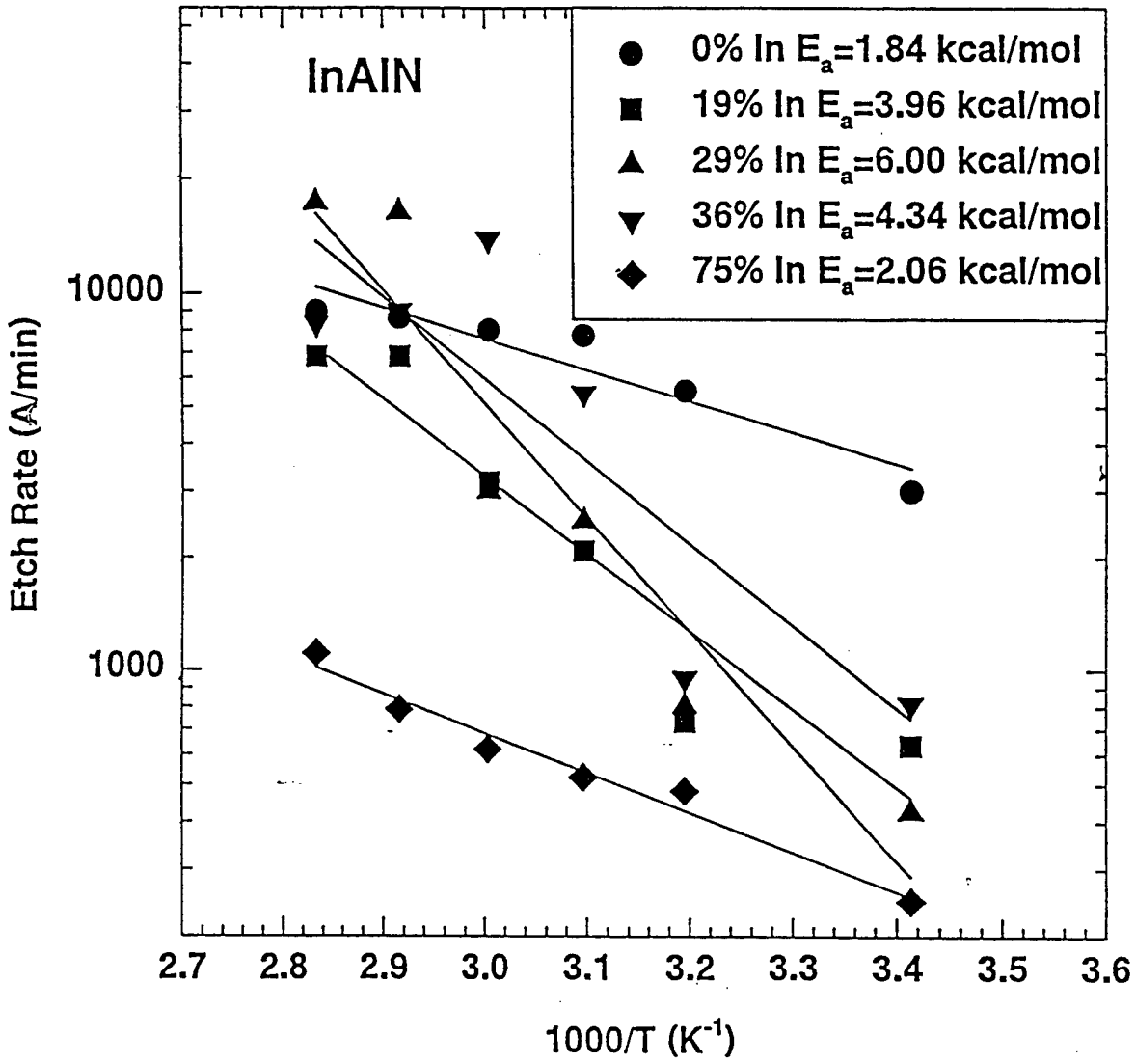

Figure 6. Arrhenius plots of etch rates for $In_XAl_{1-X}N$ for $0 \leq x \leq 1$ as function of reciprocal etch temperature, giving activation energy for etch.

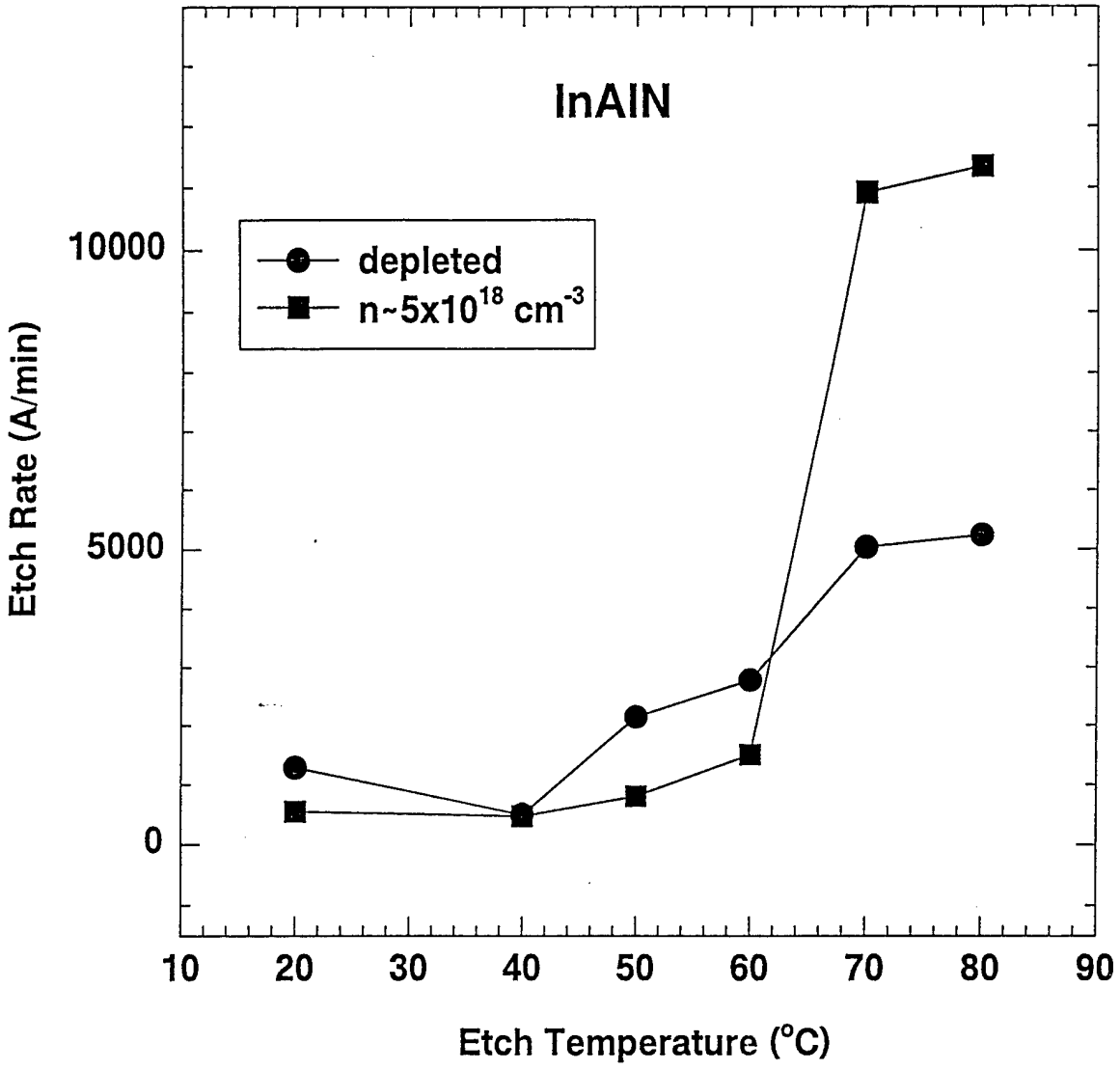

Figure 7. Etch rate for *n*-type (3.1% In) and depleted InAlN (2.6% In) as a function of solution temperature.

Dry Etch Chemistries

Two new plasma chemistries for dry etching of nitrides, ICl and IBr, have been developed. The etch rates as a function of plasma composition for GaN, InN, InAlN, AlN and InGaN are shown in Figure 8. Microwave power was held at 1000 W and rf power at 150 W (corresponding to a dc self-bias of –170 V at the sample position). For the ICl based etch (Figure 8, top), the GaN and InGaN etch rates rise as the amount of ICl in the etch increased from 12.5% to 50%, and then level off. Above 50% ICl, there appears to be a competition between the formation of $GaCl_3$ which has a boiling point of 201°C, with that of GaI_3 which sublimes at 345.[4] The $GaCl_3$ may form preferentially at some plasma compositions. The InN shows a sharp increase in etch rate above 25% ICl. This suggests that at 25% ICl the InI_3, which is much more volatile ($InCl_3$ boils at 600°C, InI_3 at 210°C.), can form easily. The InAlN and AlN are not greatly effected by changes in the composition of the plasma in ICl (or IBr, Figure 8, bottom), perhaps because both Al containing etch products have similar volatility ($AlCl_3$ boils at 183°C, $AlBr_3$ at 263°C, and AlI_3 at 191°C) and because the etch rate is probably limited by the initial bond breaking in the Al-containing materials. We expect that AlN and InAlN will be difficult to etch because of their high average bond energies (11.52 eV/atom for AlN, 7.72 eV/atom for InN, compared to 6.52 eV/atom for GaAs.[5] The N containing etch products are much more volatile than the group-III etch products, with NCl_3 boiling at <71°C while NI_3 is explosive.

The etch rates for InN and InGaN increased as the amount of IBr in the etch increased from 12.5% to 25%, and remained constant at higher percentages (Figure 8, bottom). This suggests that above 25% IBr the etching is no longer reaction-limited. The $InBr_3$ etch product is much less volatile than InI_3, as mentioned earlier. Above that composition however, there may have been competition between the formation of $InBr_3$ and InI_3, which slowed the etch, or the etch may have been limited by the removal of the reactants from the surface. GaN etch rates showed little change with IBr composition to 50% IBr plasma composition, but at 100% IBr the etch rates increased sharply. There may not have been enough reactants at the etch surface at 50% IBr, or at these lower percents of IBr there may be a competition between the formation of $GaBr_3$ and GaI_3.

In figure 8, the etch rate as a function of microwave power for GaN, InN, InAlN, AlN and InGaN is shown for values between 400 and 1000 W for ICl/Ar plasmas (top) and IBr/Ar (bottom). The rf power was held at 150 W, and 4 sccm ICl or IBr/4 sccm Ar gas flows were used. Both InAlN and AlN have low etch rates in ICl/Ar, and show no significant change in etch rate with increasing microwave power. This indicates that they are not reaction limited in this chemistry, since increasing the microwave power results in a higher concentration of reactive species which enhances the chemical component of the etch mechanism. GaN and InGaN showed a slight increase in etch rate from 400 W microwave power to 600 W. Thereafter, the GaN etch rate dropped gradually with increasing microwave power, while the InGaN etch rate dropped sharply at 800 W and then remains constant at 1000 W. This would indicate either a diffusion-limited etch, where the number of reactants becoming available exceeds the rate at which the iodine and/or chlorine etch products can be removed, or competition between reactants occurring above 600 W microwave power. The InN had a maximum in etch rate at 800 W ECR power. This might result from the large difference in volatilities of the etch

products for this material, leading to a strong sensitivity of reactant density. We expect that below that density the etch rate is reaction limited and above it there is competition between the reactants that limit the etch rate. A similar trend is observed for InN and the IBr/Ar mixtures although the peak is not as distinct.[6]

The etch rates for InAlN and AlN were again quite low in IBr based plasmas (Figure 9, bottom). GaN had constant etch rates for powers between 400 and 800 W in the IBr chemistry, and then increased sharply at 1000 W. The InGaN etch rate again decreased with increasing microwave power. As the InGaN etch rate increased monotonically with increasing rf power (as will be seen shortly), the removal of the etch products would seem to be limiting the etch rates for this material.

In Fig. 10, the rms roughness for GaN etched in ICl/Ar as a function of rf power is shown along with the roughness for the as-grown sample. These samples were unpatterned to avoid roughness caused by redeposition of mask material. The etched surfaces were significantly smoother than that of the as-grown sample indicating that surface features are removed predominantly by sputtering. Sharp features will be removed by ion milling faster that flat features because of the angular dependence of removal rates.

Figure 11 shows the etch selectivity of GaN over InN, InAlN, InGaN or AlN under ICl/Ar conditions as a function of rf power (top), percent ICl (middle) and microwave power (bottom). The selectivity of GaN over the other nitrides rose with increasing rf power, with GaN/AlN reaching ~6 and GaN/InAlN almost 5 at 250 W rf. The volatility of the $InCl_3$ was lower than that of $GaCl_3$, and as the percent ICl in the etch increased, so did the selectivity for GaN/InN, reaching ~10 at 100% ICl. With both $GaCl_3$ and GaI_3 having high volatilities, with increasing reactant concentration, GaN was etched faster than the In-containing compounds, which may still be limited by the removal of $InCl_3$. GaN etch much faster than AlN and InAlN as well for most microwave powers (Figure 11, bottom), achieving selectivities of ~8 and 5, respectively, at 600 W microwave power. In IBr/Ar chemistries, the selectivities were low, as shown in Figure 12, never going above 4 for any set of rf or microwave powers of plasma compositions. We assume this is due to the similar volatilities of iodide and bromide etch products.

In summary, the etch rates for GaN, InN, InAlN, AlN and InGaN were measured in ICl/Ar and IBr/Ar plasmas. The sensitivity to changes in plasma chemistry, microwave power, and rf power appears to be directly influenced by the volatility of the group-III –I and Cl- or Br-etch products. InN, with the largest difference between volatility of etch products, proved to be the most sensitive to the plasma composition and ion density in ICl/Ar plasma chemistries. Very fast etch rates were achieved for GaN, InN and InGaN in ICl/Ar chemistries. At 250W, rf power, AlN and InAlN had slow etch rates in this mixture and were affected very little by changes in etch conditions. GaN and AlN etched in IBr/Ar showed a sharp increase in etch rate as the IBr composition increased from 50% to 100%, while the etch rates for the other materials stayed relatively constant above 25% IBr. All the materials showed a general increase in etch rate with increasing rf power in both chemistries. The etched surface of GaN under both plasma chemistries was found to be extremely smooth with little preferential loss of N from the surface at low rf powers. There was no detectable residue from the etch chemistry.

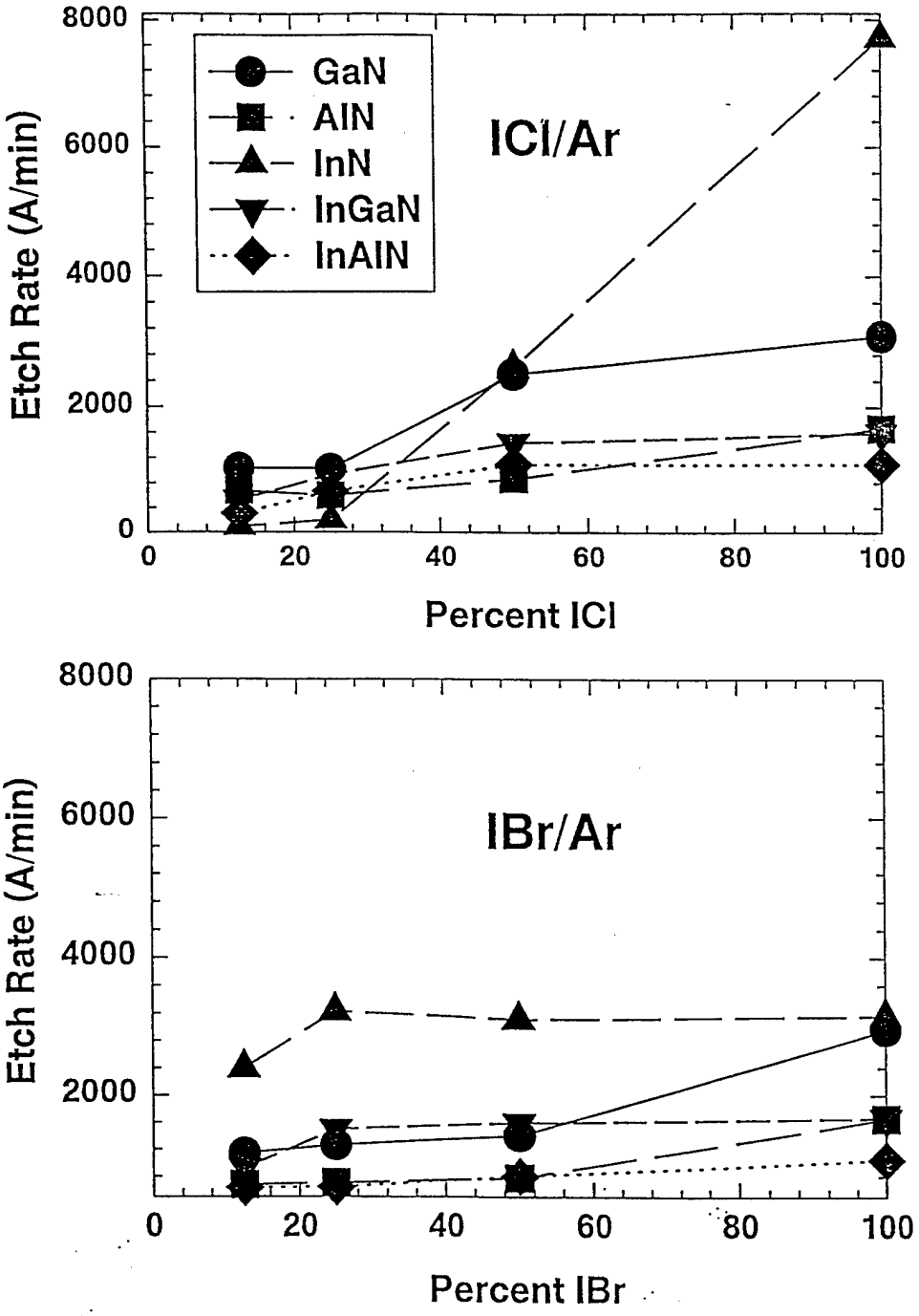

Figure 8. Etch rate as a function of percent ICl (top) or IBr (bottom) for GaN, InN, InAlN, AlN and InGaN in 1000 W (ECR), 150 W rf 1.5 mTorr discharges.

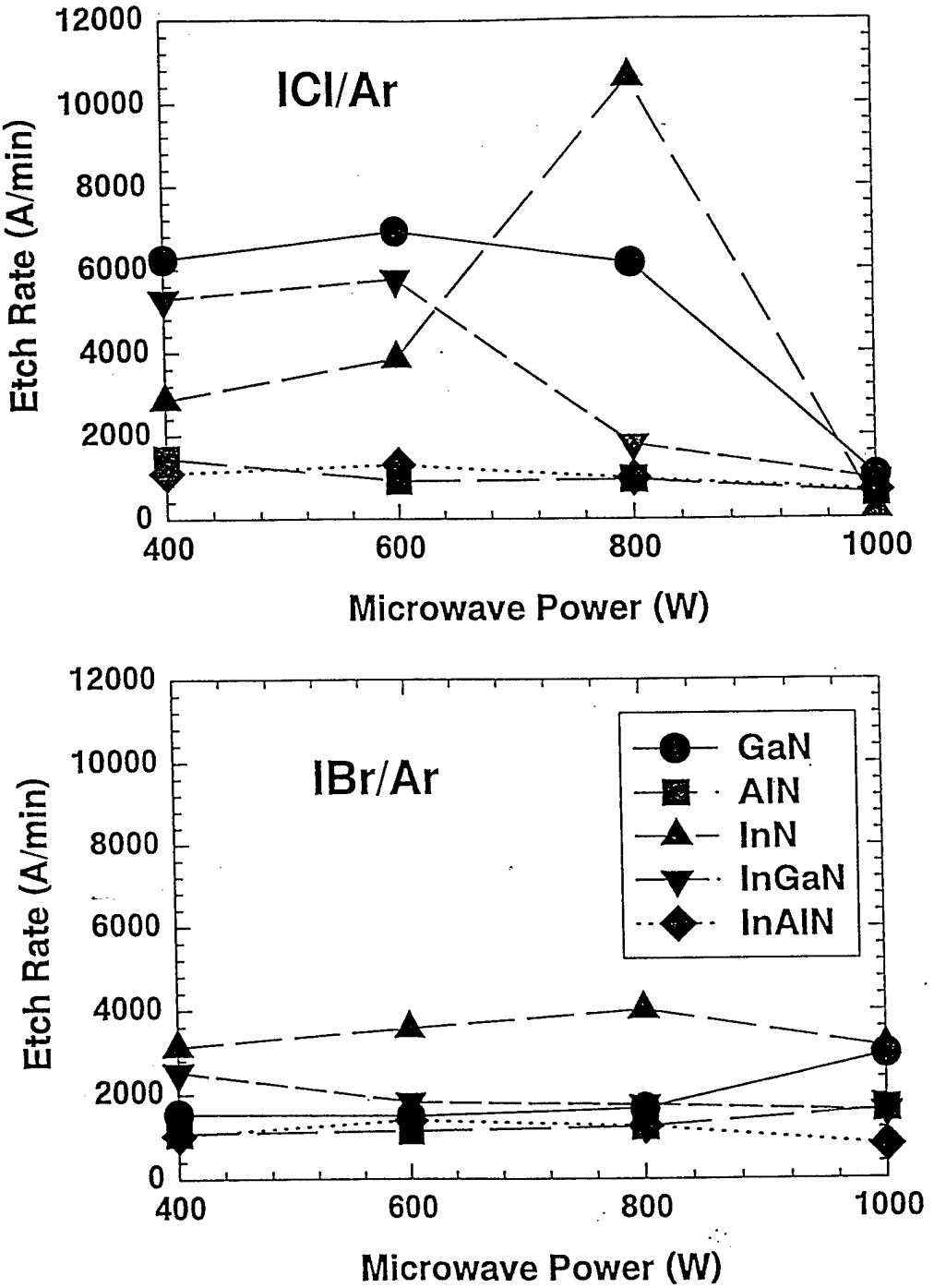

Figure 9. Etch rate as a function of microwave power for GaN, InN, InAlN, AlN and InGaN in 4ICl/4Ar (top) or 4IBr/4Ar (bottom) plasmas (150 W rf, 1.5 mTorr).

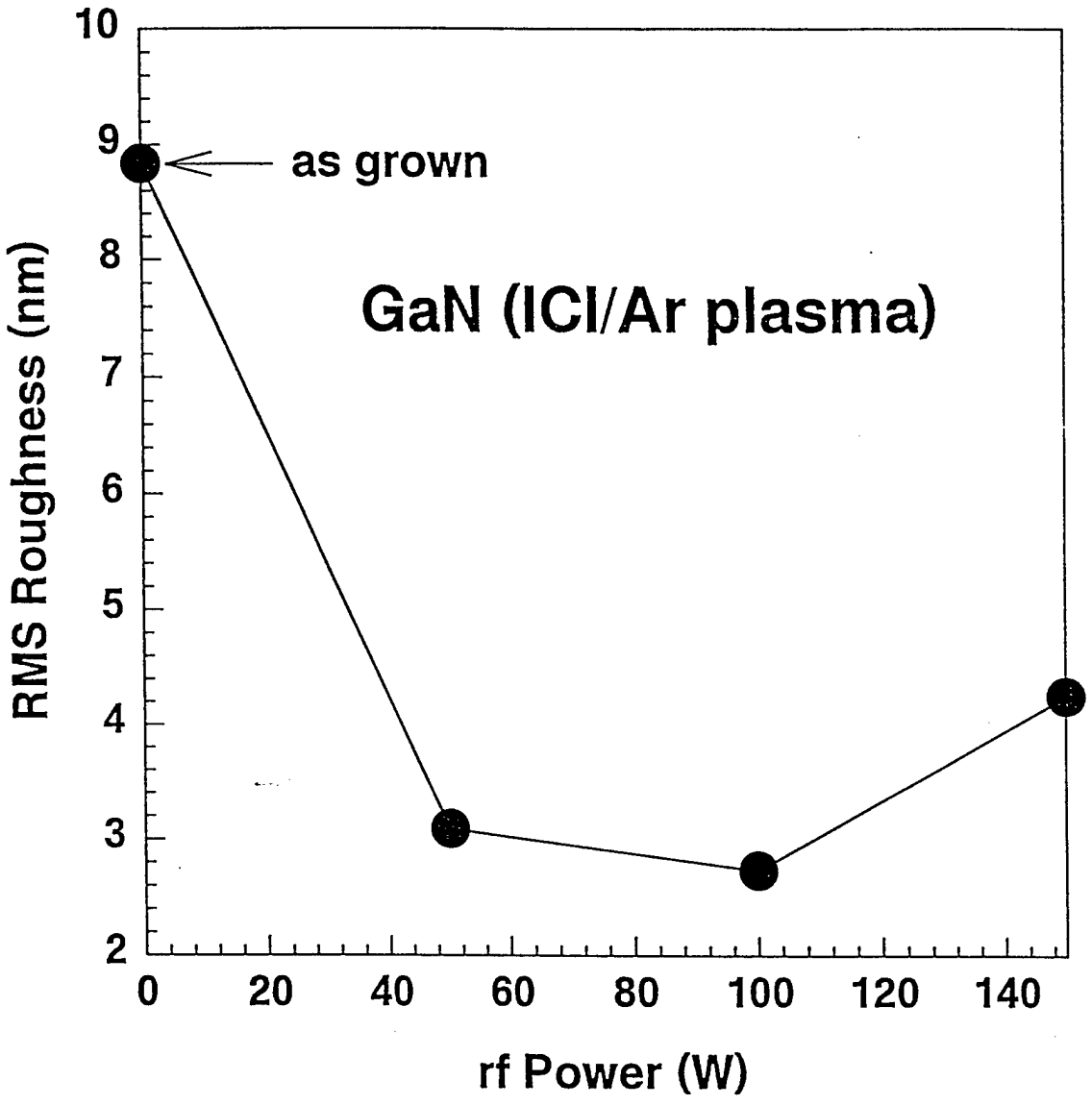

Figure 10. rms roughness for GaN as a function of rf power in 4ICl/4Ar 1000 W ECR, 1.5 mTorr discharge plasmas.

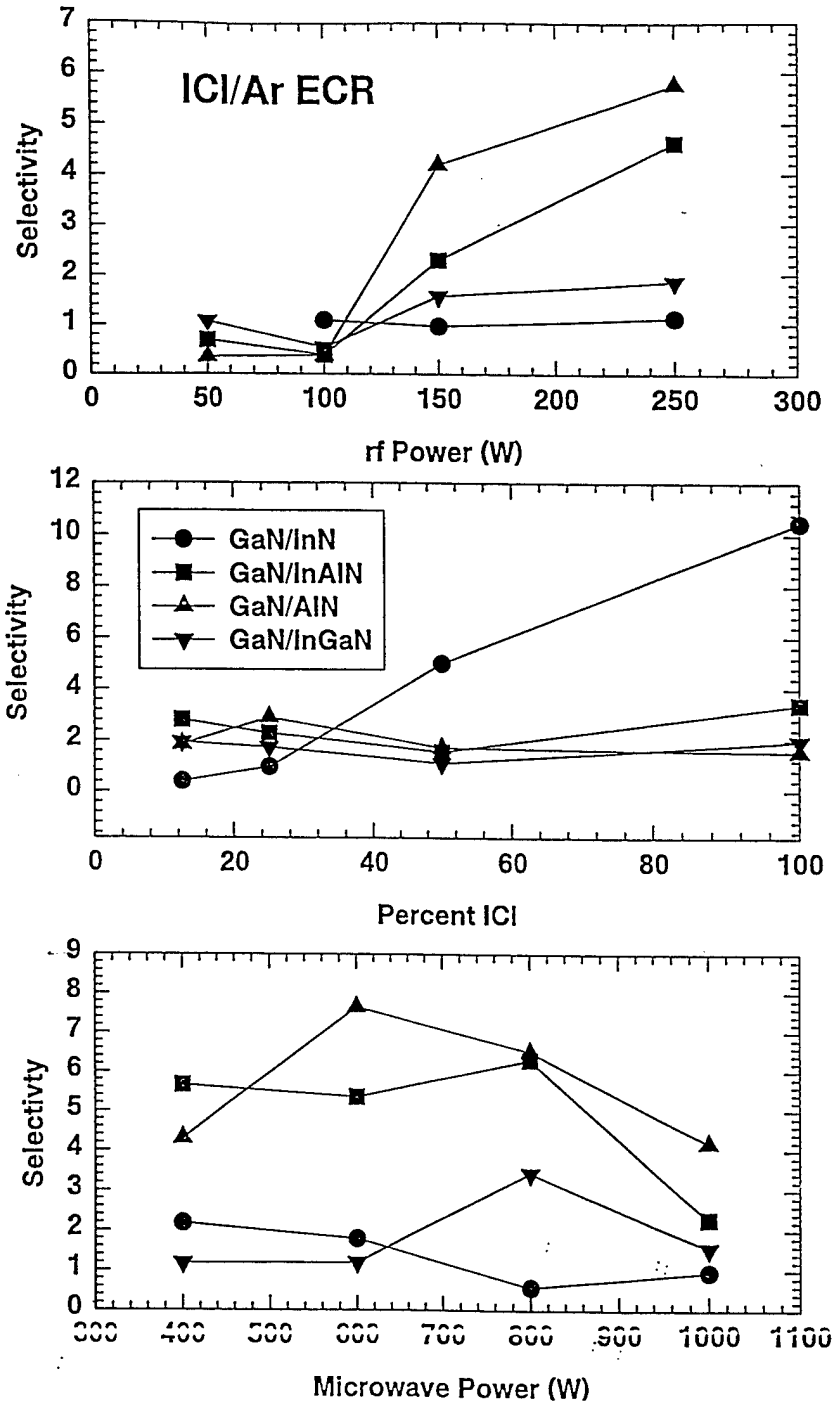

Figure 11. Selectivity of GaN over InN, InAlN, InGaN or AlN in ICl/Ar plasmas as a function of rf power (top), percent ICl (middle) and microwave power (bottom). The ECR power was 1000 W for the top two plots, the rf power 150 W for the bottom two plots, and the plasma composition 4ICl/4Ar for the top and bottom plots.

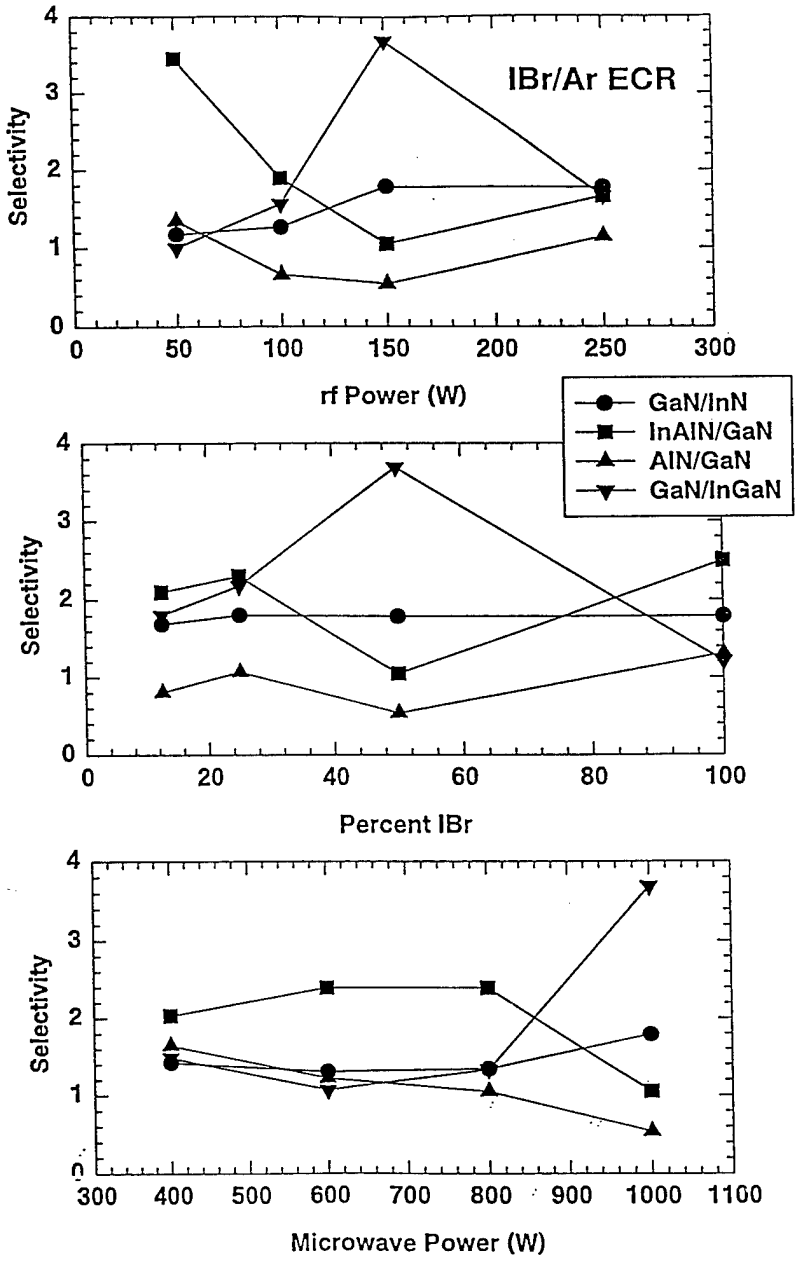

Figure 12. Selectivity of GaN over InN, InAlN, InGaN or AlN under IBr/Ar plasmas as a function of rf power (top), percent ICl (middle) and microwave power (bottom). The ECR power was 1000 W for the top two plots, the rf power 150 W for the bottom two plots and the plasma composition 4ICl/4Ar for the top and bottom plots.

Dry Etching Using Inductively Coupled Plasma Sources

High density plasma systems have demonstrated much higher etch rates for the III-nitrides than conventional reactive ion etch systems, because of the efficiency of the high ion flux in breaking the bonds in the material. Most of this work has been performed with electron cyclotron resonance (ECR) reactors, but a more attractive option is inductively coupled plasma (ICP). The advantages of ICPs in brief include improved uniformity, more mature turning networks and lower cost-of-ownership.

Figure 13 shows that at fixed dc self-bias (-100 V) and plasma composition ($10Cl_2/5Ar$), increasing the ICP source power increases the nitride etch rates by increasing the ion flux and the atomic chlorine density (the latter measured by actinometry). The results for InN are similar to what we observe for InP in that there is a sharp rise in etch rate above a particular source power, which we ascribe to the prevention of formation of an $InCl_3$ selvedge layer which normally retards further etching. Further increases in flux (corresponding to source powers above 1000 W) do not increase the InN (or InAlN) etch rate, which at that point may be limited by Cl arrival at the surface. The other materials show a general trend of increasing etch rate across the entire range of ICP source powers.

It is expected that to reduce the currently high contact resistance in GaN-based heterostructure field effect transistors, and eventually heterojunction bipolar transistors, InN-based contact layers will be necessary, in analogy to InGaAs on GaAs. In this case, the ability to selectively etch InN relative to the other nitrides will be crucial. Typical selectivities for InN over GaN and AlN are 0.5-10.

Figure 14 (top) shows the influence of applied rf chuck power on nitride etch rate at fixed source power (750 W) and pressure (2 mTorr). The same basic trend is observed for all of the materials, namely an initial increase as ion energy is increased (from ~25 eV at 25 W chuck power, to ~80 eV at 100 W chuck power), followed by a decrease above a particular chuck power. This type of behavior is somewhat common in high density plasma dry etching of III-V materials, and is usually ascribed to ion-enhanced removal of the active chlorine species from the semiconductor surface before they can react, if the ion energy exceeds a particular value, which depends on ion flux. Selectivities for etching InN relative to the other nitrides are shown in the lower part of Figure 14, and again show values <10 under all conditions.

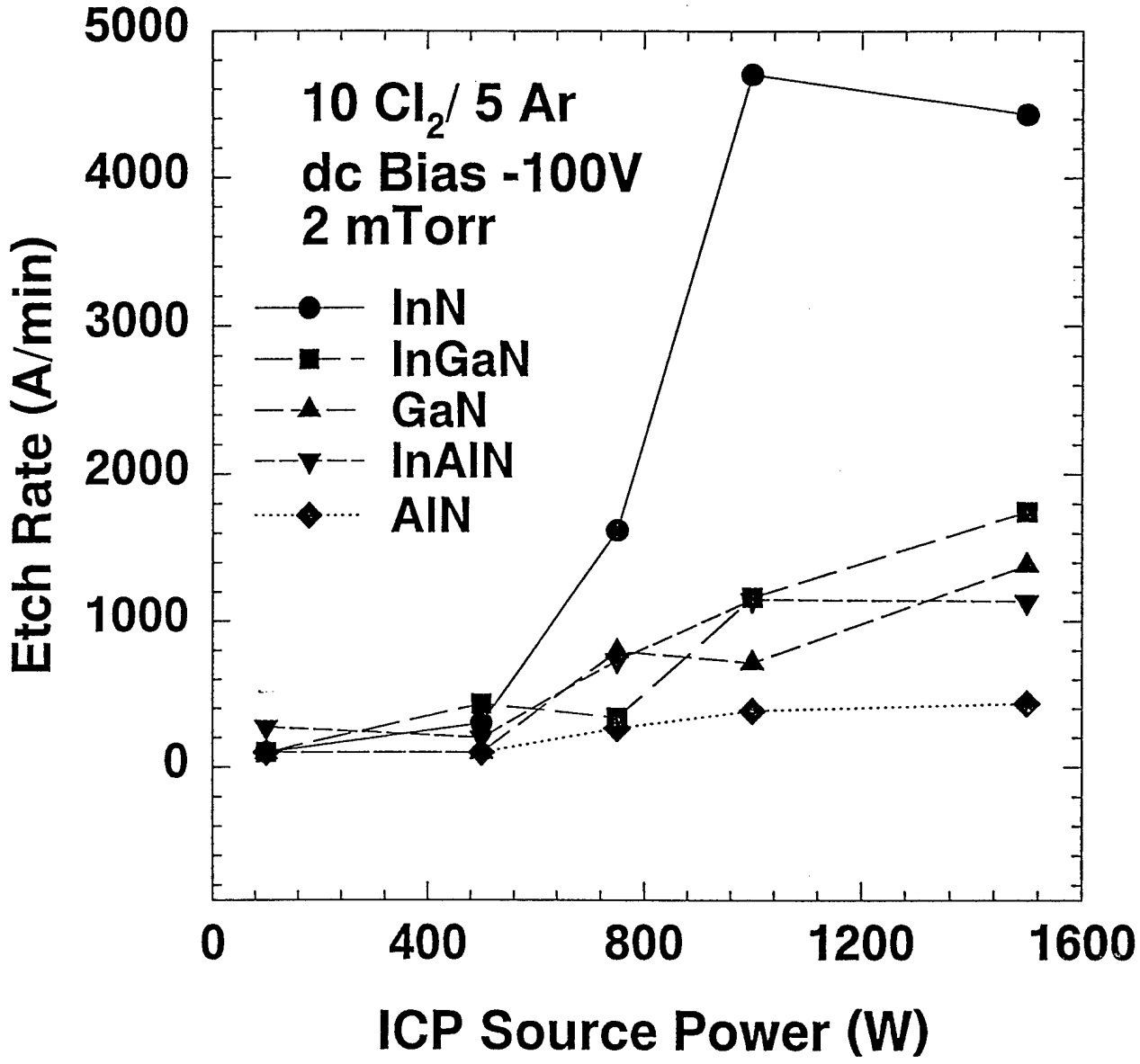

Figure 13. Etch rates of III-nitrides in $10Cl_2/5Ar$ discharges (- 100 V dc self-bias, 2 mTorr) as a function of source power.

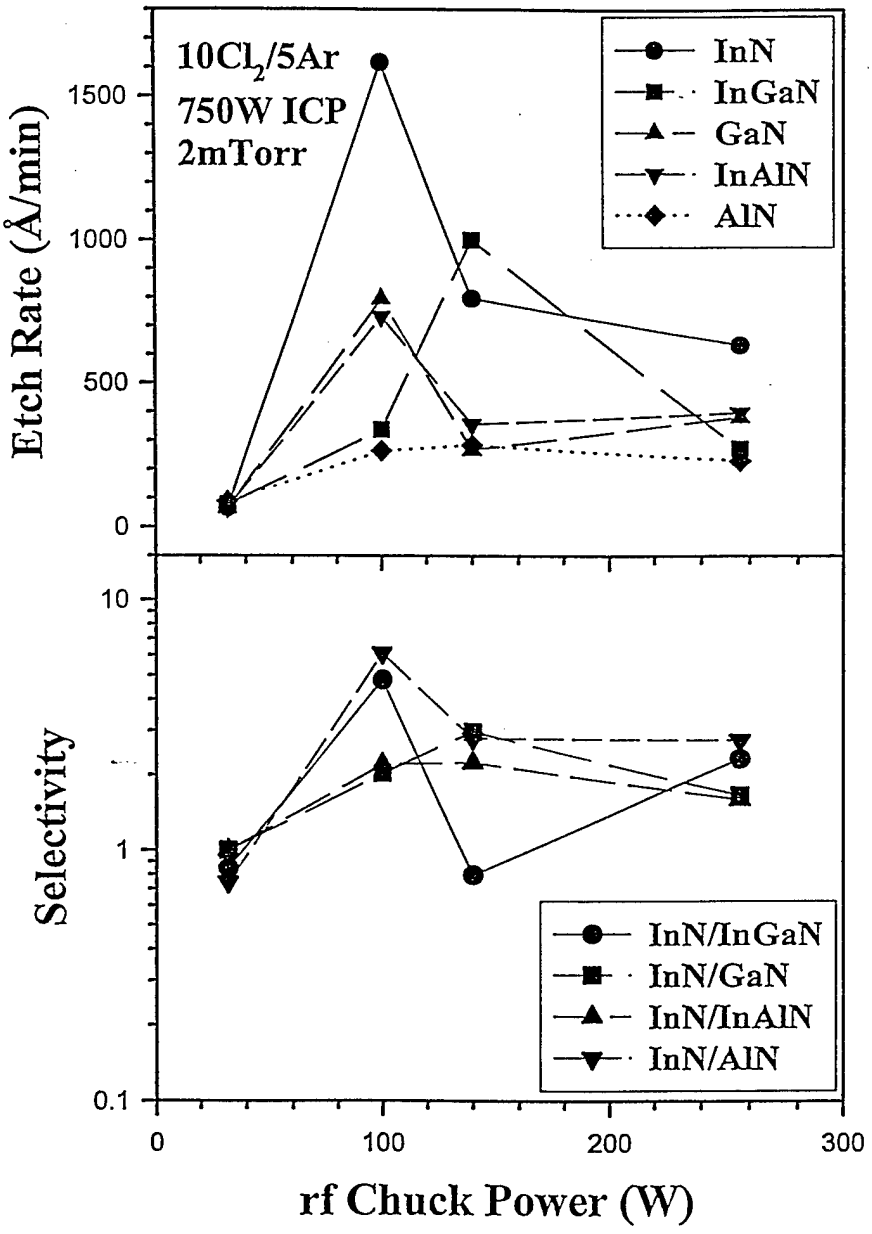

Figure 14. Etch rates (top) and selectivities for InN over the other nitrides as a function of rf chuck power in Cl_2/Ar ICP discharges.

The evolution of GaN surface morphology with rf chuck power was measured by AFM. The unetched control material had root-mean-square (rms) surface roughness of ~8 nm over a $10x10\mu m^2$. The etched surface morphologies were strong functions of both plasma composition and rf chuck power, but almost independent of source power. Figure 15 shows the variation of rms value with both rf chuck power (top) and percentage Cl_2 in the discharge (bottom). It appears that at least some reasonable ion energy (i.e. 50-100 eV) is necessary to promote smooth morphologies (and even some degree of surface smoothing through the angular dependence of etch rate on initially relatively rough surfaces such as nitrides), but above a threshold energy there is roughening due to preferential sputtering of N, as reported by Shul et.al.[7] for ECR etching. As seen in the lower part of Figure 15, pure Ar discharges produce significant surface roughening, due most likely to preferential sputter ion of the higher N atoms. As Cl_2 is added to the discharge the morphology initially improves, due to the formation of volatile group III chlorides (expected to be predominantly $GaCl_3$ under these conditions) that lead to a less disparate rate removal of Ga and N from the surface. However, at higher Cl_2 compositions there is increased surface roughening which again may result from reaction of non-stoichiometry surfaces.

The rates are highest at low pressure where ion-assisted desorption is most efficient (Figure 16), and with Ar addition which produces the best conditions for etch product removal relative to the lighter N_2^+ and H_2^+ ions (Figure 17).

Figure 18 shows the etch rate for GaN, AlN, InN, InGaN and InAlN as a function of dc bias at 500 W ICP power (top) and 1000 W ICP power (bottom) in $CH_4/H_2/Ar$ plasmas. The pressure was held at 2 mTorr. For the same applied rf chuck power, the dc bias was higher at lower ICP power. This is due to the higher plasma density, which suppresses the cathode dc self-bias at higher ICP powers.

In Figure 19, etch rates for GaN, AlN, InN, InGaN and InAlN are shown as a function of ICP power at 150 (top) and 350 W rf chuck power (bottom) in $CH_4/H_2/Ar$ plasmas at 2 mTorr. The dc bias at each source power is also shown. At 150W rf power (dc bias range from -405 V at O W ICP to –29 V at 1500 W ICP), the etch rate increased with increasing ICP power. This indicates that the etch was reaction limited under these conditions, with the etch rate increasing with increasing plasma density, irrespective of the decreasing ion energy. At 350 W rf chuck power, the etch rates initially increased rapidly as the ICP power was increased from 0 to 500 W. The dc bias was higher under these conditions, ranging from –645 V at 0 W ICP to –58 V at 1500 W ICP power. At 500 W ICP power the etch rates were up to four times faster at the higher rf power (350 W). The GaN etch rate fell sharply above 500 W ICP power, while the etch rates of the In-containing materials increased to 750 W ICP power and then fell off. The etch would appear to no longer be reaction limited above the particular powers at which the etch rates are a maximum. Rather, bond breaking and removal of the etch products may be limiting the ion-assisted etch rate due to the lower ion energies, or the reactive gas phase species $(CH)_X$ are dissociated at the higher plasma sources.

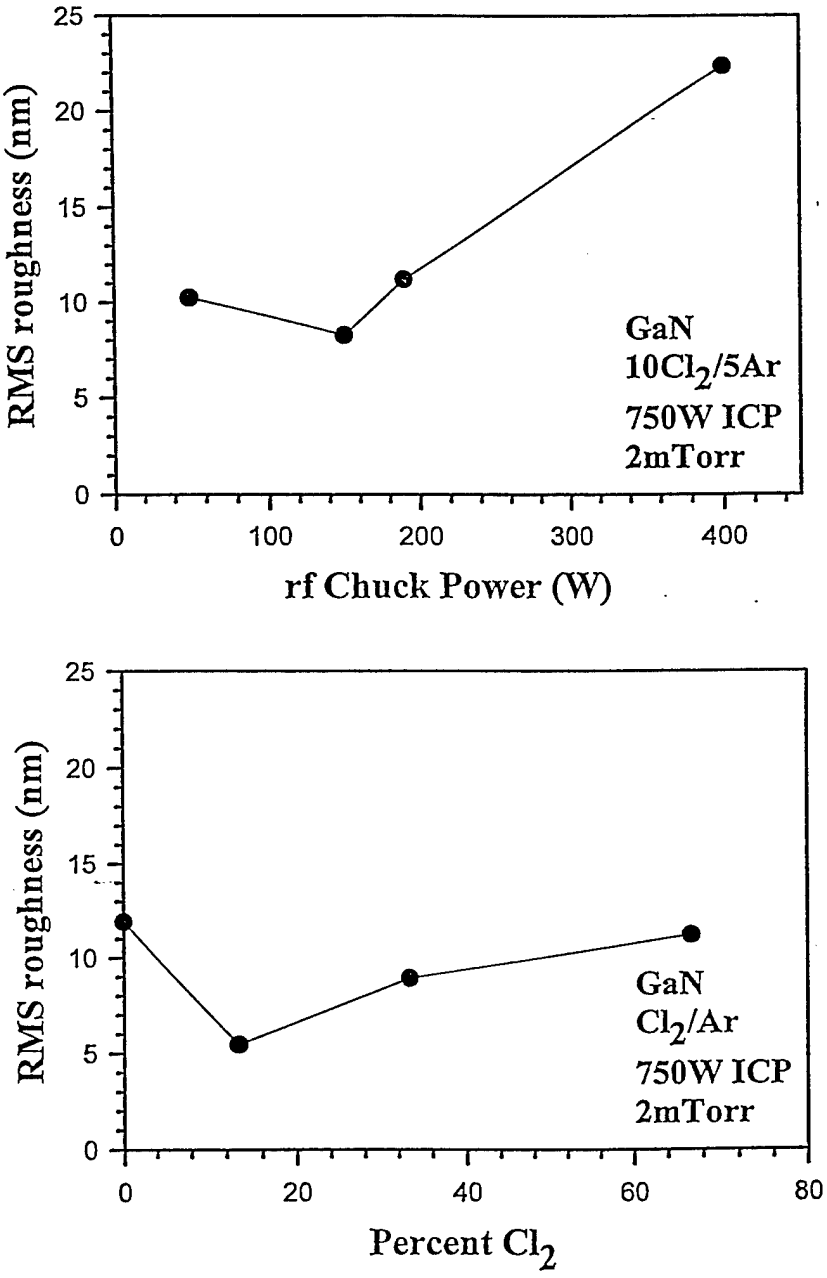

Figure 15. RMS surface roughness of GaN after etching in Cl_2/Ar ICP discharges as a function of (top) rf chuck power or (bottom) discharge composition at affixed rf chuck power of 190 W.

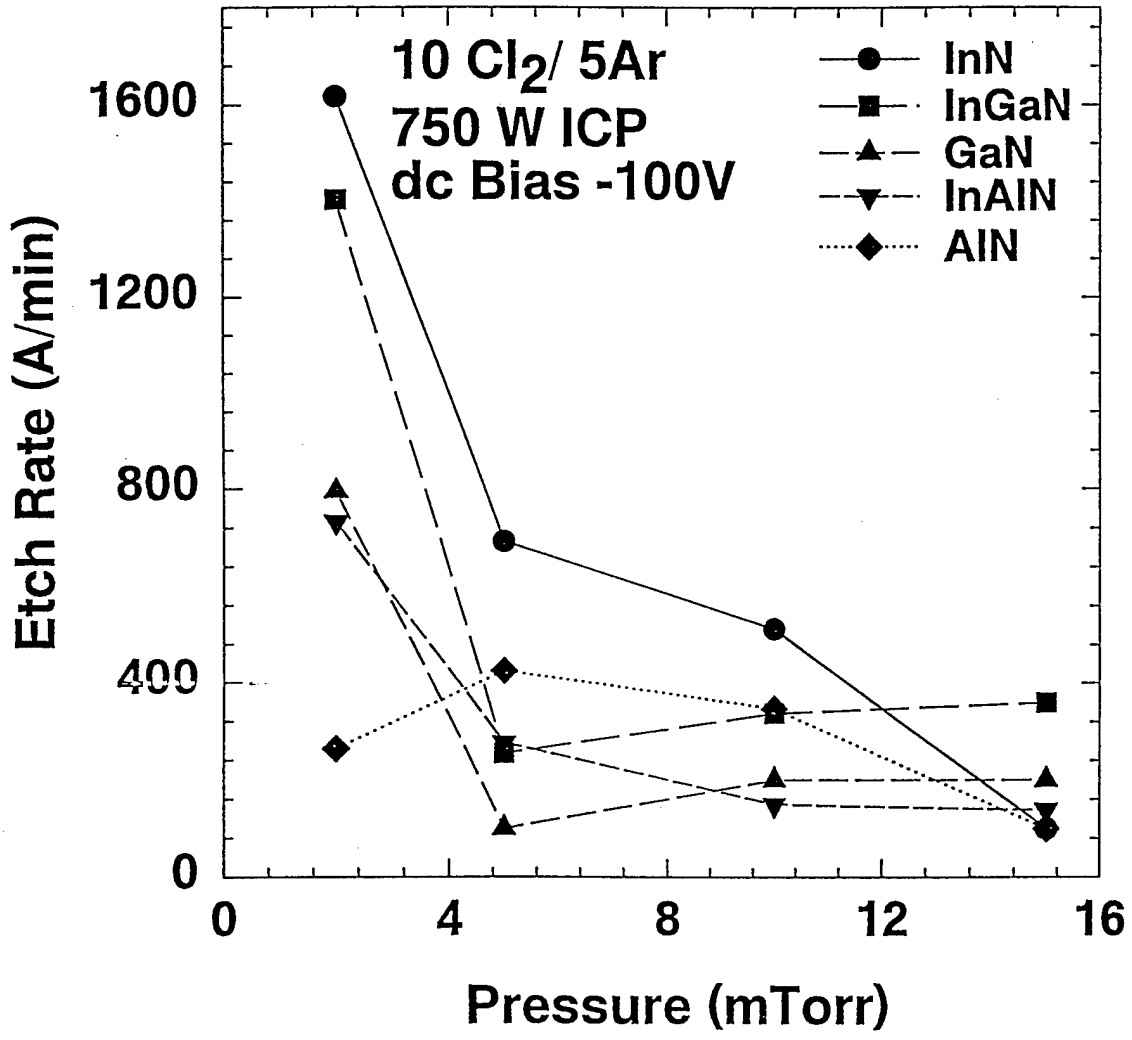

Figure 16. Nitride etch rates as a function of pressure in ICP/Cl_2/Ar discharges.

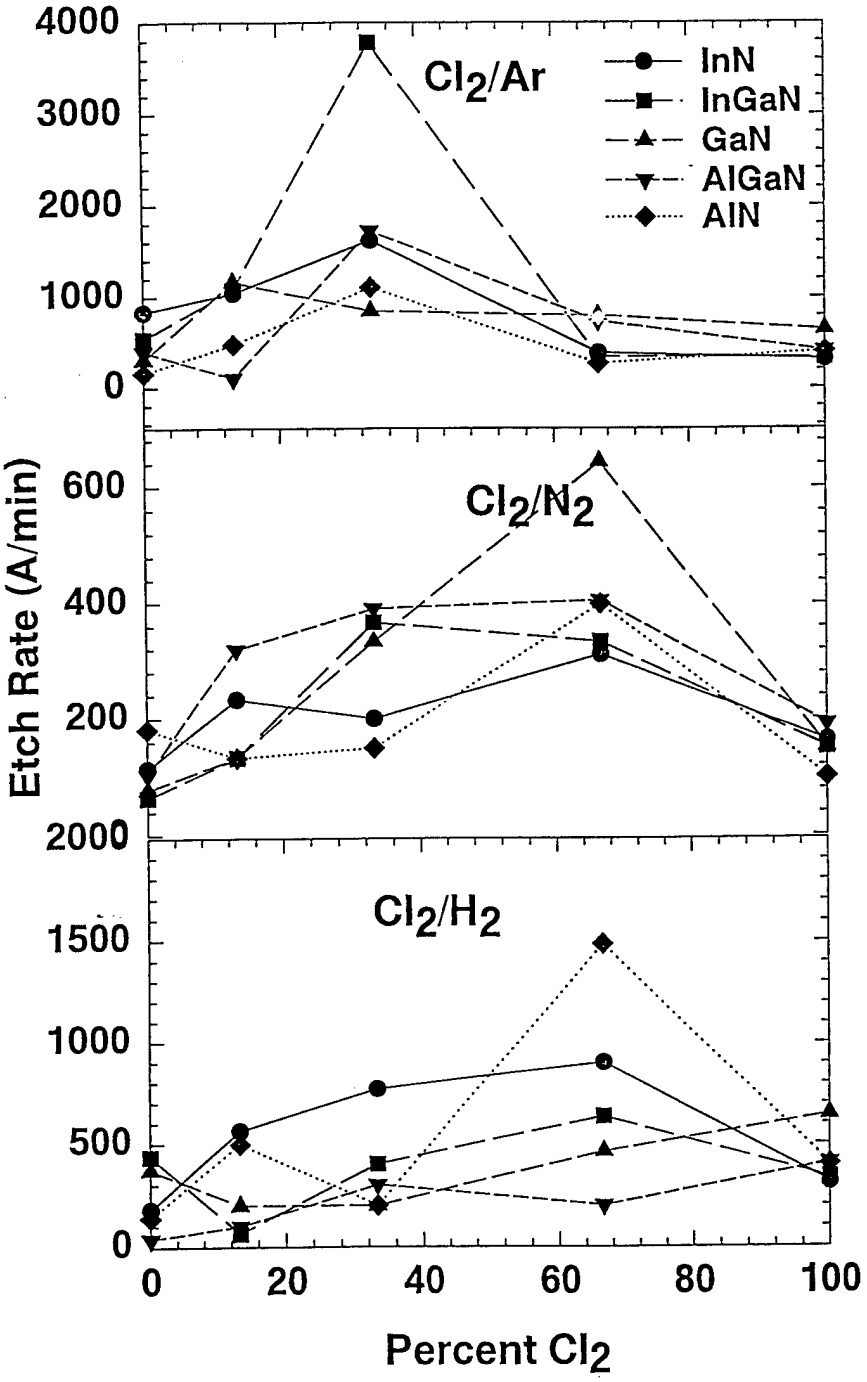

Figure 17. Comparison of nitride etch rates in Cl_2/Ar, Cl_2/H_2 and Cl_2/N_2 ICP discharges.

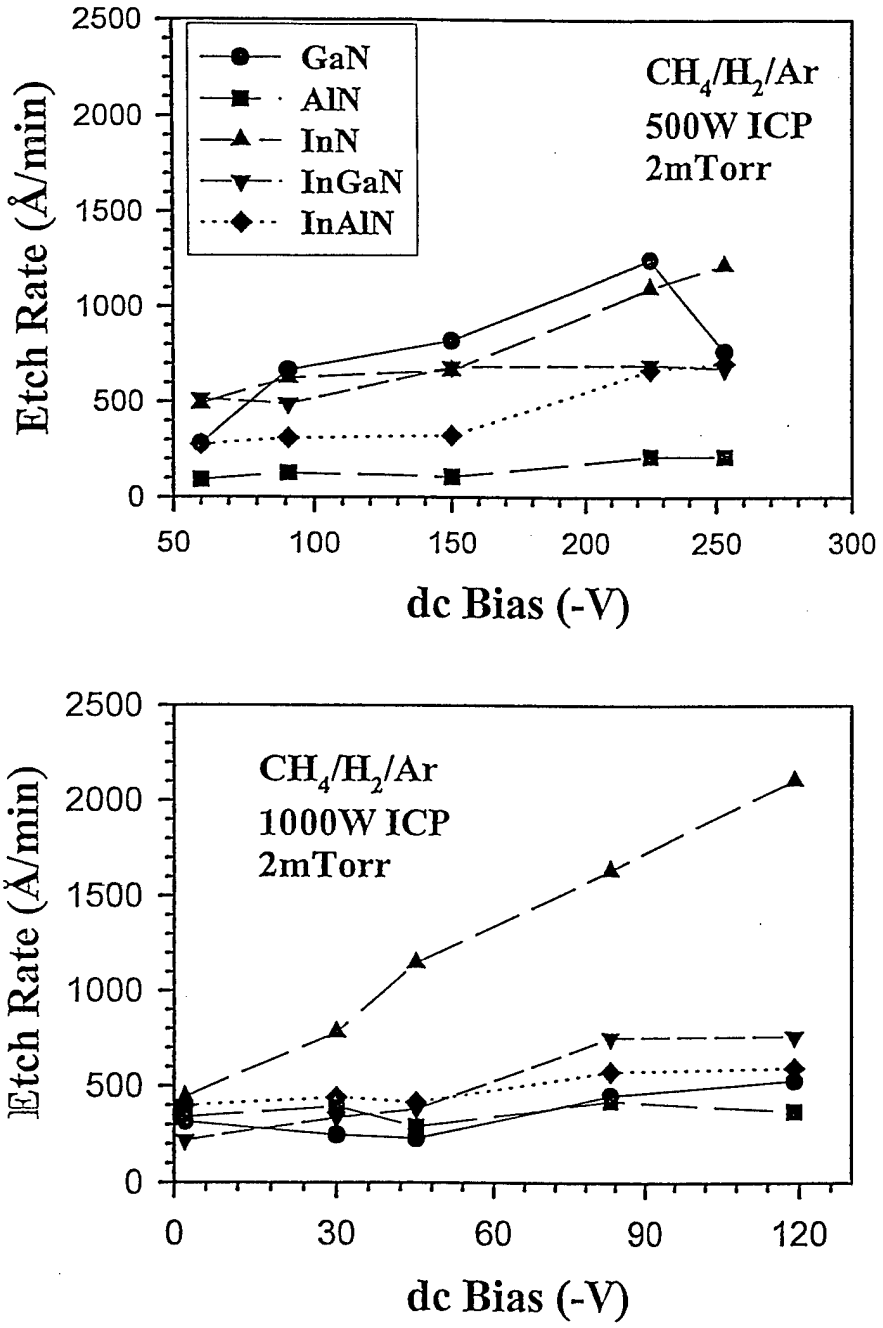

Figure 18. Etch rates for III-nitrides as a function of dc-self bias at either 500 W (top) or 1000 W (bottom) ICP source power, in 2 mTorr $CH_4/H_2/Ar$ discharges.

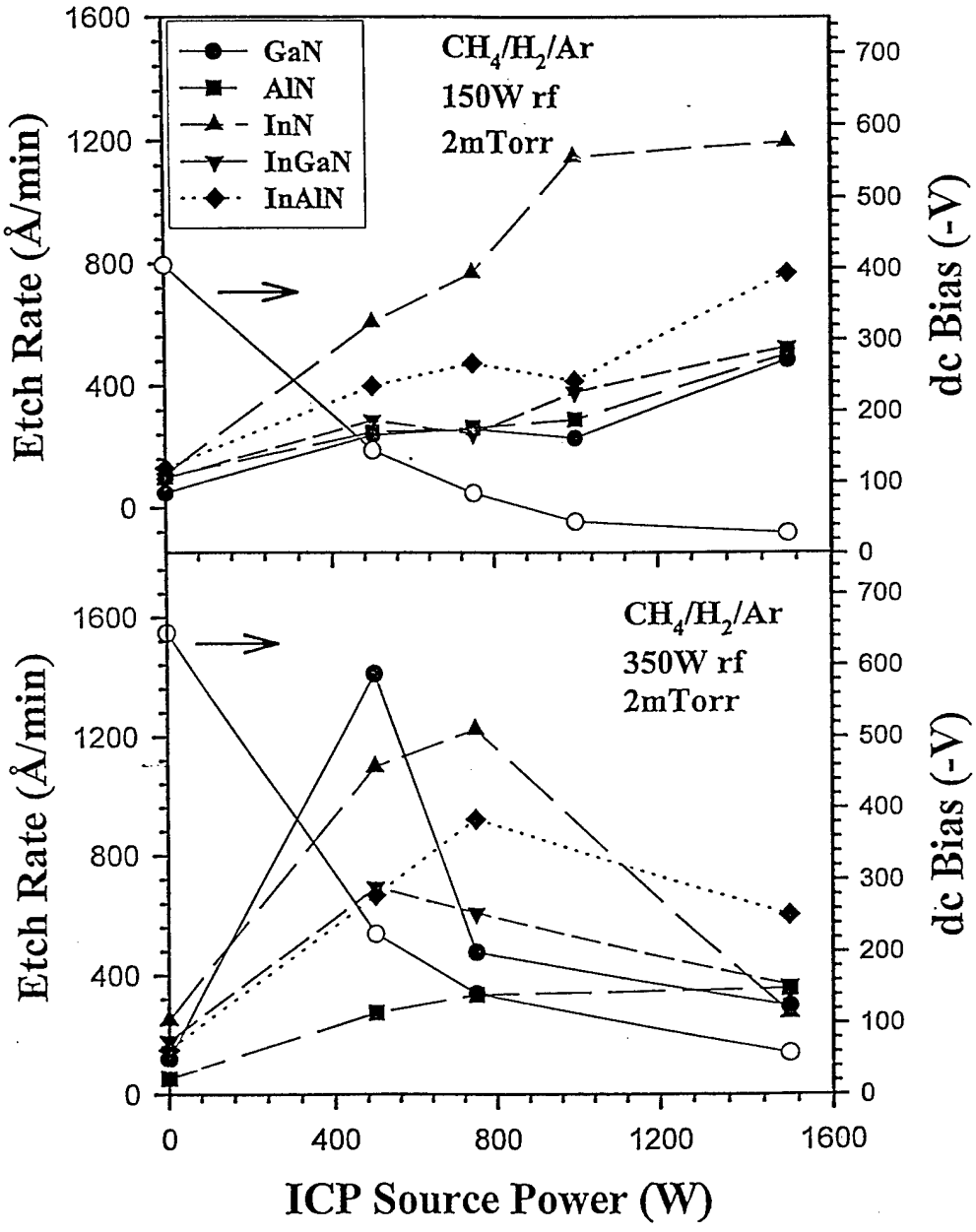

Figure 19. Etch rates for III-nitrides as a function of ICP source power at either 150 W (top) or 350 W (bottom) rf chuck power, in 2 mTorr $CH_4/H_2/Ar$ discharges.

Inductively coupled plasma etching with Cl_2 or CH_4/H_2 discharges is able to produce practical etch rates for the III-nitride materials (i.e. 500-1500Å min^{-1}) at low dc self-biases (-100 V), where conventional reactive ion etching is impractically slow. The rates are a strong function of the discharge composition, pressure and both source power and rf chuck bias. Vertical sidewalls are obtained over the entire range of conditions investigated, due to the ion-assisted nature of the etching. For Cl_2 etching, the etched surface morphology of GaN is smoothest at low Cl_2-to-Ar ratios (~1:5-10). In this chemistry, maximum etch selectivity of ~6 was obtained for InN over the other nitride materials -- this is basically a result of its lower bond energy (7.72 eV/atom compared to 8.92 eV/atom for GaN and 11.52 eV/atom for AlN), because the volatility of $InCl_3$ is substantially lower than either $GaCl_3$ or $AlCl_3$ or $AlCl_3$. For CH_4/H_2 etching, the rates increase with bias and ion flux, except at high rf power in the latter case. Good anisotropy is also possible in CH_4/H_2 because of the ion-driven etch mechanism.

The root-mean-square (rms) roughness as a function of ICP power for GaN in $CH_4/H_2/Ar$ plasmas at 150 W rf power and 2 mTorr showed that the etched surfaces were all smoother than the as-grown sample. This may be because sharp features tend to be etched faster due to the angular dependence of ion milling, and as long as there is not preferential loss of nitrogen from the surface, the rms roughness may decrease. The smoothest surface was found at 500 W ICP power. The low roughness would indicate that there was little preferential loss of the group V species from the surface, though this needs to be verified by Auger electron spectroscopy (AES). The basic trend is that the surfaces are smoother at lower ion energy conditions. Figure 20 shows the raw AFM data for GaN as-grown and after etch as a function of ICP power in $CH_4/H_2/Ar$ plasmas.

Figure 21 shows the selectivities of etch for InN over GaN, AlN, InGaN and InAlN in $CH_4/H_2/Ar$ plasmas as a function of dc bias (top) and ICP power (bottom). As the dc bias increased, the selectivity for InN over AlN increased. The bond strength of InN is much less than that of AlN (7.7 and 11.5 eV, respectively), which indicates that the ions were able to break the bonds in the InN material more efficiently as their energy increased but did not have sufficient energy to efficiently break the bonds in AlN. The selectivity of InN over GaN also rose initially with increasing dc bias for the same reason. Above –55 V, however, the ions had enough energy to efficiently remove GaN (bond strength of 8.9 eV) as well, lowering the selectivity of the etch. The selectivities of InN over InGaN and InAlN were less than three under all conditions. Both InN/GaN and InN/AlN showed a maxima in the plot at 1000 W ICP power (Figure 21, bottom). The dc bias decreased with increasing ICP power. As the plasma density increased, the etch rates of both AlN and GaN increased, while the accompanying decrease in ion energy leads to the etch rate of InN remaining approximately constant. SEM micrographs of features etched into AlN (top) and InN (bottom) using $CH_4/H_2/Ar$ ICP plasmas are shown in Figure 22.

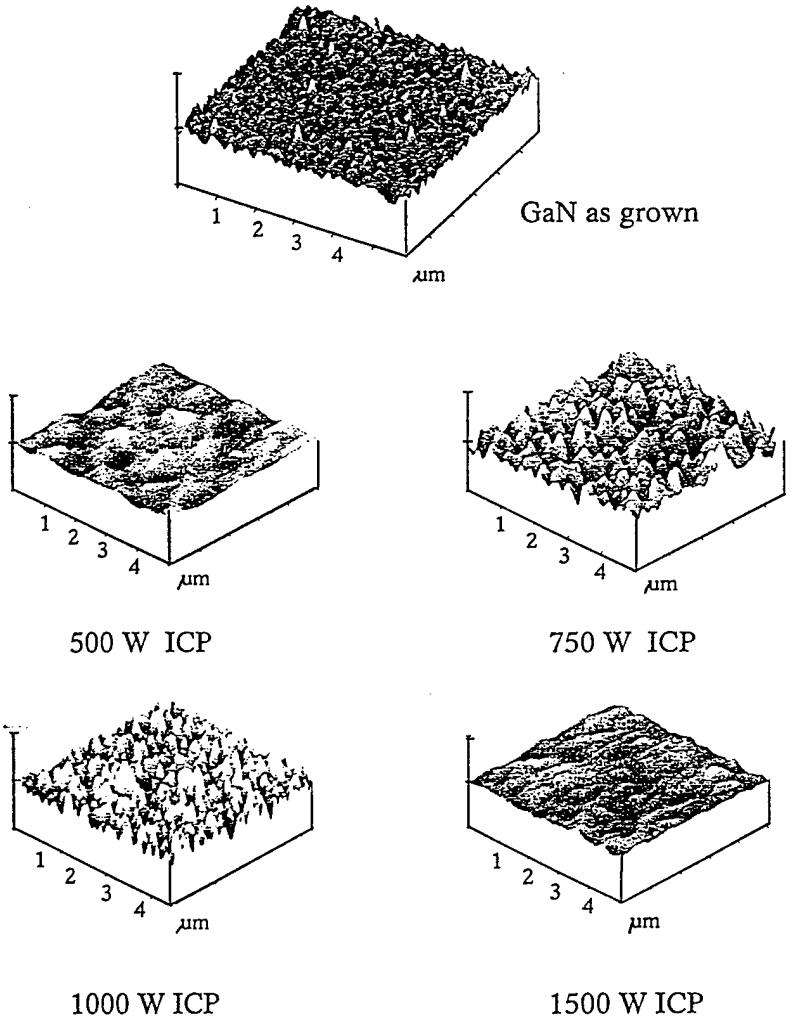

Figure 20. Raw AFM data showing surfaces of GaN as-grown and after etch as a function of ICP power in $CH_4/H_2/Ar$ plasmas at 2 mTorr and 150 W rf power. The vertical scale is 1000Å per division.

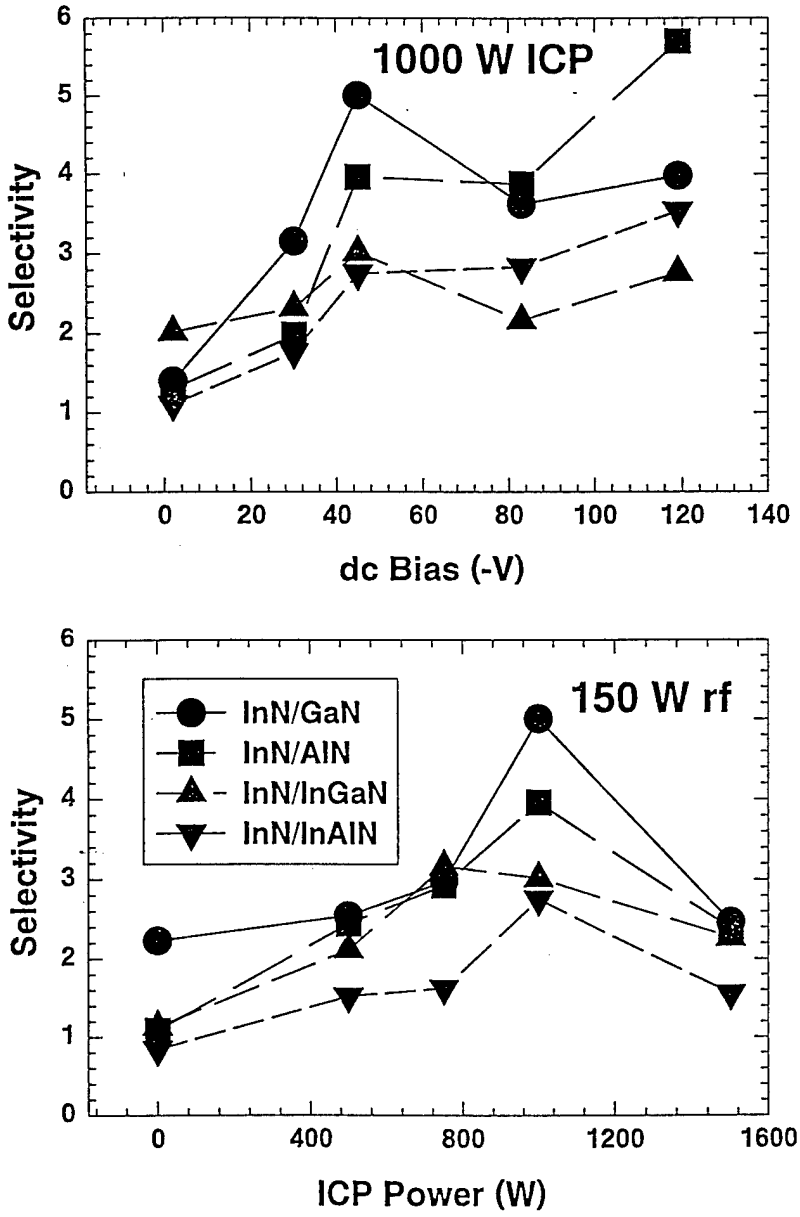

Figure 21. Selectivities at 2 mTorr for InN over GaN, AlN, InGaN and InAlN in $CH_4/H_2/Ar$ plasmas as a function of dc bias (top) and ICP power (bottom).

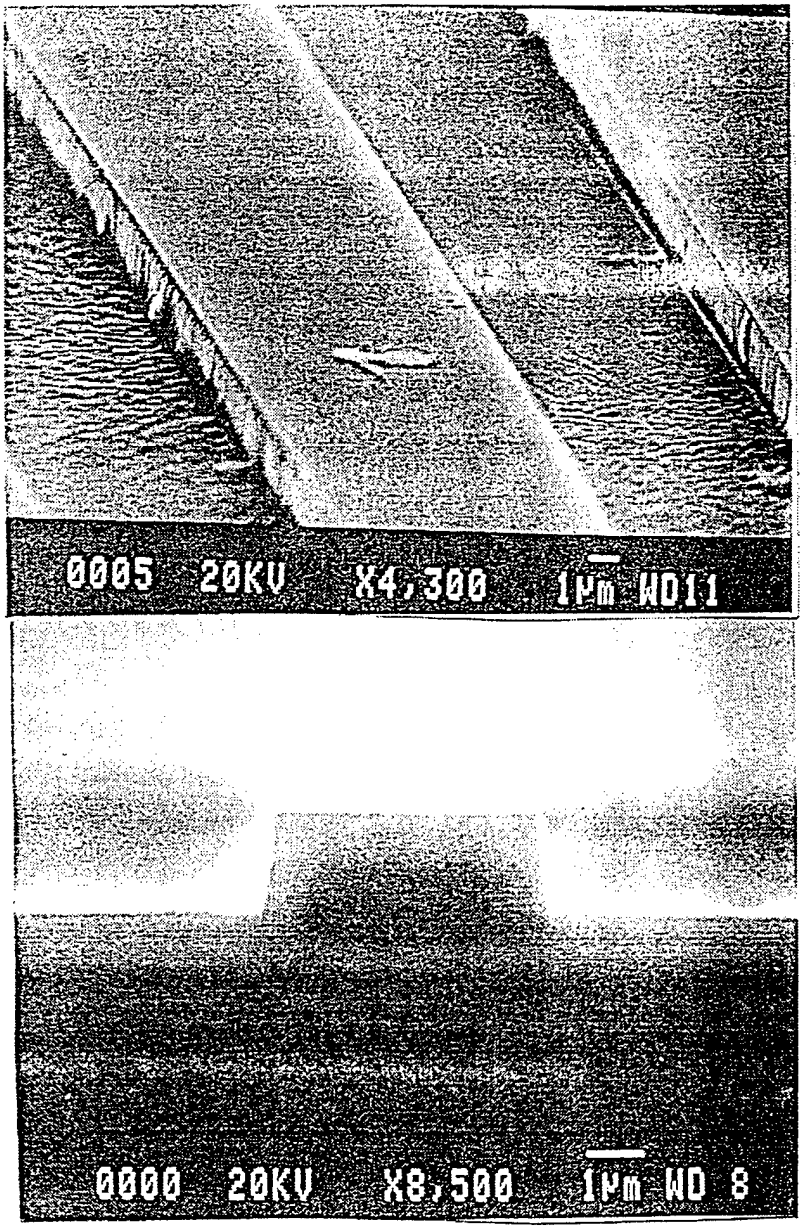

Figure 22. SEM micrographs of features etched in AlN (top) and InN (bottom) with ICP $CH_4/H_2/Ar$ plasmas.

Effect of Dry Etching on Optical Properties

Increasing the ion energy in a plasma etch system typically results in highly anisotropic, high rate etching due to the physical sputter desorption of the etch products. However, bombardment of semiconductor surfaces with energetic ions generated during plasma etching can damage the near surface region and produce lattice damage if the ions energy are greater than the displacement energy of the host atoms. As these energetic ions strike the sample, damage as deep as 100 nm can occur[8], causing degradation of device performance. This damage can include simple Frenkel pairs consisting of a vacancy and the displaced atom, implanted etch ions, broken bonds, formation of dangling bonds, or deposition. Attempts to minimize the damage by reducing the ion energy below the damage threshold for compound semiconductors (<40 eV)[9] or by increasing the chemical component of the etch results in more isotropic profiles, significantly limits minimum dimensions, and reduces the etch rate. It is therefore necessary to develop plasma etch processes which couple high etch rates, anisotropy, and sidewall profile control with low-damage for optimum device performance.

Since GaN is more chemically inert that GaAs and has higher binding energies, higher ion energies may be used during the etch with potentially less damage to the material. However, reports of plasma-etch-induced-damage of the group-III nitrides has been limited. We have found that for InN, InGaN, and InAlN exposed to an ECR-generated plasma the damage increased as a function of ion flux and energy.[10] ICP etching offers an attractive alternative etch technique which may be easier to scale-up than ECR sources, and may be more economical in terms of cost and power requirements. ICP plasmas are formed in a dielectric vessel encircled by an inductive coil into which rf-power is applied. A strong magnetic field is induced in the center of the chamber which generates a high-density plasma due to the circular region of the electric field that exists concentric to the coil. At low pressures (≤10 mTorr), the plasma diffuses from the generation region and drifts to the substrate at relatively low ion energy. Thus, ICP etching is expected to produce low damage while achieving high etch rates. In this section, we eport on ICP and ECR plasma-induced-damage of GaN as a function of rf-power and source power. Pure Ar plasmas were used to simulate the ion bombardment conditions created during plasma etching of the group-III nitrides.

The GaN samples used in this study were grown by metal organic chemical vapor deposition (MOCVD) on a c-plane sapphire substrate in a multiwafer rotating disk reactor at 1040°C with a 20 nm GaN buffer layer grown at 530°C.[11] The GaN film was approximately 1.8μm thick. The ECR plasma reactor used in this study was a load-locked Plasma-Term SLR 770 etch system with a low profile Astex 4400 ECR source in which the upper magnet was operated at 165 A. Energetic ion bombardment was provided by superimposing an rf-bias (13.56 MHz) on the sample. Etch gases were introduced through an annular ring into the chamber just below the quartz window. To minimize field divergence to optimize plasma uniformity and ion density across the chamber, an external secondary collimating magnet was located on the same plane as the sample and was run at 25 A. The ICP reactor was a load-locked Plasma-Therm SLR 770 etch system with a Plasma-Therm ICP source. The reactor was a cylindrical coil configuration with a ceramic vessel encircled by a 3-turn inductive coil into which the rf-power (2 MHz) was applied. Identical to the ECR, energetic ion bombardment was

provided by superimposing an rf-bias (13.56 MHz) on the sample. Etch gases were introduced through an annular region at the top of the chamber. Unless otherwise mentioned, ECR and ICP etch parameters used in this study were: 40 sccm of Ar, 30°C electrode temperature, 1 mTorr total pressure, 500W of applied source power, and 1 to 250W rf-power with corresponding dc-biases of -10 to -300± 25V.

All samples were mounted using vacuum grease on an anodized Al carrier that was clamped to the cathode and cooled with He gas. Samples used to measure PL intensity were 5mm x 5mm and unpatterned. Samples used to calculate etch rates were patterned using AZ 4330 photoresist. Etch rates were calculated from the depth of etched features measured with a Dektak stylus profilometer after the photoresist was removed with an acetone spray. Each sample was approximately 1 cm^2 and depth measurements were taken at a minimum of three positions. Standard deviation of the etch depth across the sample was nominally less than ± 10% with run-to-run variation less than ± 10%. Root-mean square (rms) surface roughness was quantified using a Digital Instruments Dimension 3000 atomic force microscope (AFM) system operating in tapping mode with Si tips.

PL measurements were made at liquid helium temperature (10 K) in a continuous flow cryostat. A HeCd laser (325 nm) was used as the excitation source and the typical excitation power was 5 mW. The detection system consisted of a 0.275 meter spectrometer in conjunction with a thermoelectrically cooled UV-enhanced CCD detector. Measurements were taken using a 100 line/mm grating for high resolution data and a 150 line/mm grating for low resolution, broad spectral range data. To evaluate the effect of high temperature on the PL, samples were annealed in an Addax AET rapid thermal annealer in flowing Ar, preceded by a three cycle pump/purge sequence to reduce the background oxygen level. In the annealer, samples were contained in a SiC coated graphite crucible with thermocouples monitoring the temperature at two points on the crucible. Anneal times were 30 s at the prescribed set point ± 10°C.

Prior to the etch experiments, the two inch GaN wafer was mapped out to examine the uniformity of the PL emission. In Figure 23 we show the PL spectrum at the center of the wafer taken with the low resolution grating. The spectrum consisted of two distinct features. The dominant near band-edge resonance was seen at 3.472 eV (as verified by spectra taken with 1 meV resolution). Emission resonances in this spectral region have been identified with recombination of a neutral-donor-bound excition[12,13], was not clearly resolved. The broad spectral feature centered at approximately 2.21 eV was associated with emission from deep level impurities. The oscillations in the deep level emission were due to optical interference effects in the film. We focused on the near-band-edge emission for the majority of our etch studies.

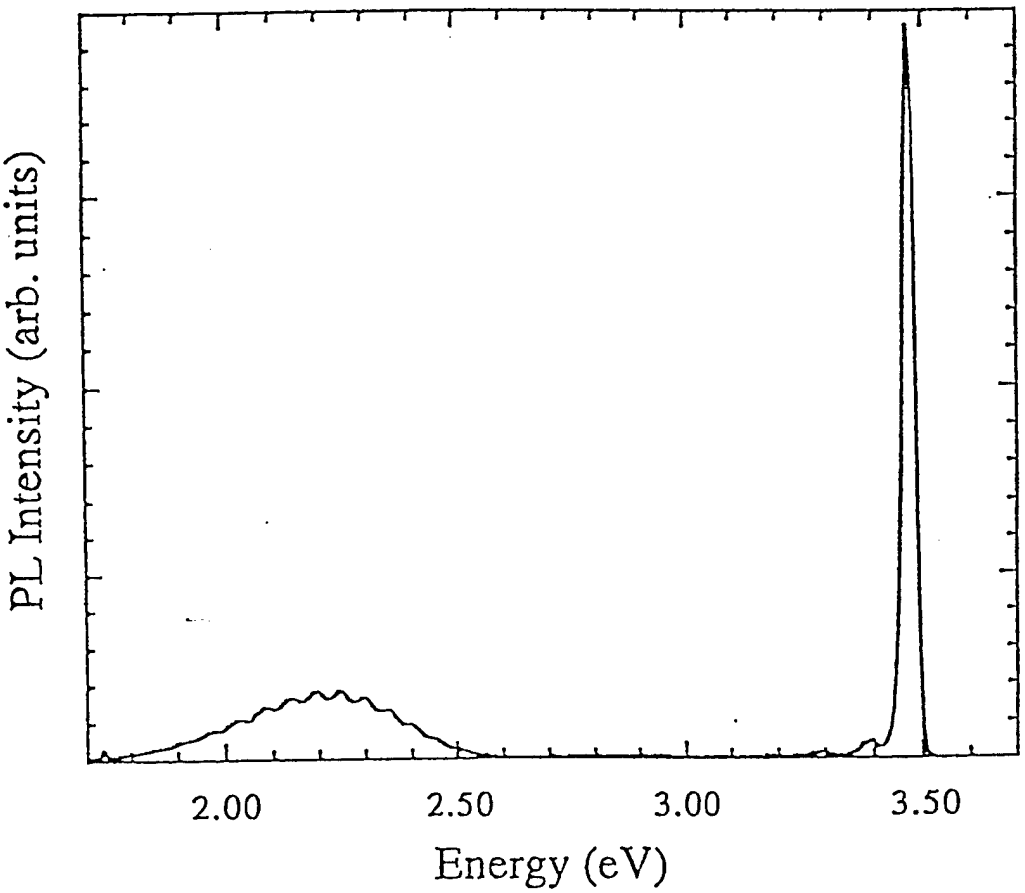

Figure 23 PL spectrum from GaN films at T=10K.

In Figure 24, we plot the peak intensity of the near-band-edge emission as a function of radial position on the two inch GaN wafer. The intensity dropped by approximately 15% at a radial position of 0.5 inches and approximately 30% at a radial position of 0.8 inches. Toward the edge of the wafer, the intensity drop was significantly more rapid. The samples that were used in the etch studies were diced from the center part of the wafer, within the 0.6 inch radial position. The PL spectra were taken before and after etching for each sample. The PL spectrum of a reference sample from the wafer was compared during each experiment to ensure consistency of the excitation conditions. The PL band-edge emission is expected to be accurate to ± 10%.

The first study evaluated the effect of rf-power on the peak near band-edge PL intensity. GaN samples were exposed to ICP- and ECR-generated Ar plasmas for 1 minute under identical plasma conditions while the rf-power was increased. The dc-bias was approximately 10 to 65% higher in the ECR under comparable conditions. In Figure 25, the percent change in the peak PL intensity versus rf-power is plotted for both ECR and ICP etching. For the ICP case, at relatively low rf-powers (1 and 50 W) the PL intensity slightly degraded, and as the rf-power was increased up to 250 W increasing degradation in PL intensity was seen. Depth profiling of similar films at a rf-power of 1 W (~10 V dc-bias) revealed no detectable material removed whereas the 250 W etch (-300 V dc-bias) resulted in GaN sputter loss of approximately 770Å during a 1 minute exposure.

Distinctly different results were obtained for etching in the ECR plasma system. As seen in the figure, etching with very low rf-power (1 W) resulted in an over 80% increase in the PL intensity and virtually no sputter loss of GaN. Etching at higher rf-powers also improved the PL intensity, but to a lesser degree as the rf-power was increased. The highest power (150 W) etch resulted in a very slight decrease in PL intensity and the sputter rate under these conditions was determined to be approximately 820Å/min.

We also studied the effect of plasma density on the peak near band-edge PL intensity. GaN samples were exposed to ICP- and ECR-generated Ar plasmas for 1 minute. The dc-bias was held approximately constant at -65 ± 15 V by varying the rf-power. The data was more scattered than the rf-power data for both ICP and ECT conditions. The ICP showed virtually no change in PL intensity at 250 W source power and then decreased by 30% as the ICP power was increased to 750 W. The PL intensity at 250 W source power was then decreased by 30% as the ICP power was increased to 750 W. The PL intensity decreased by only 10% at 1000 W ICP power which was an improvement of almost 20% over 750 W. In the ECR, we observed an increase of ~115% in PL intensity at 250 W ECR power. Similar to the trend observed as a function of rf-power, the PL intensity also improved at higher ECR powers but at a lower rate. Sputter rates for GaN were approximately 30 ± 10Å/min at 250 W source power and 225 ± 25Å/min at 1000 W. Further studies are underway to identify the effect of plasma density.

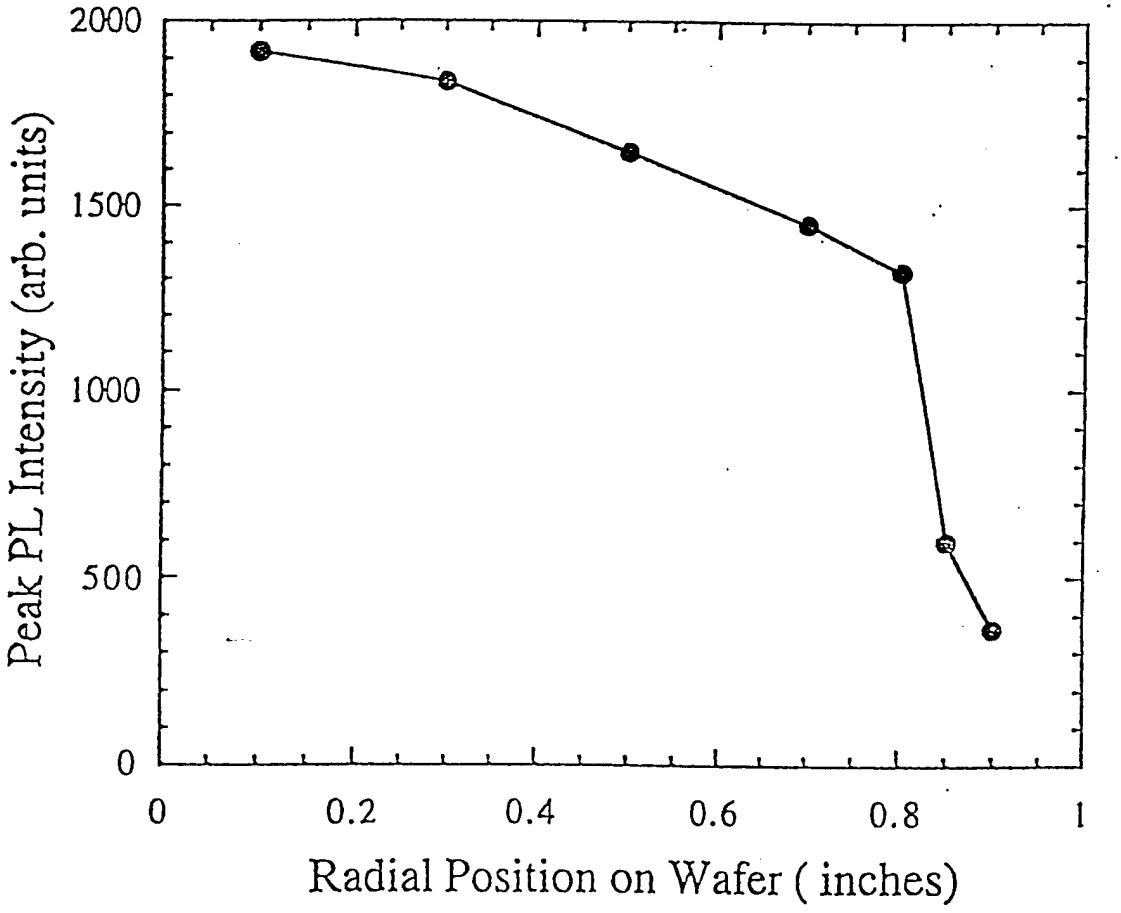

Figure 24 Variation of the peak PL intensity as a function of radial position on the two inch GaN/Al_2O_3 wafer.

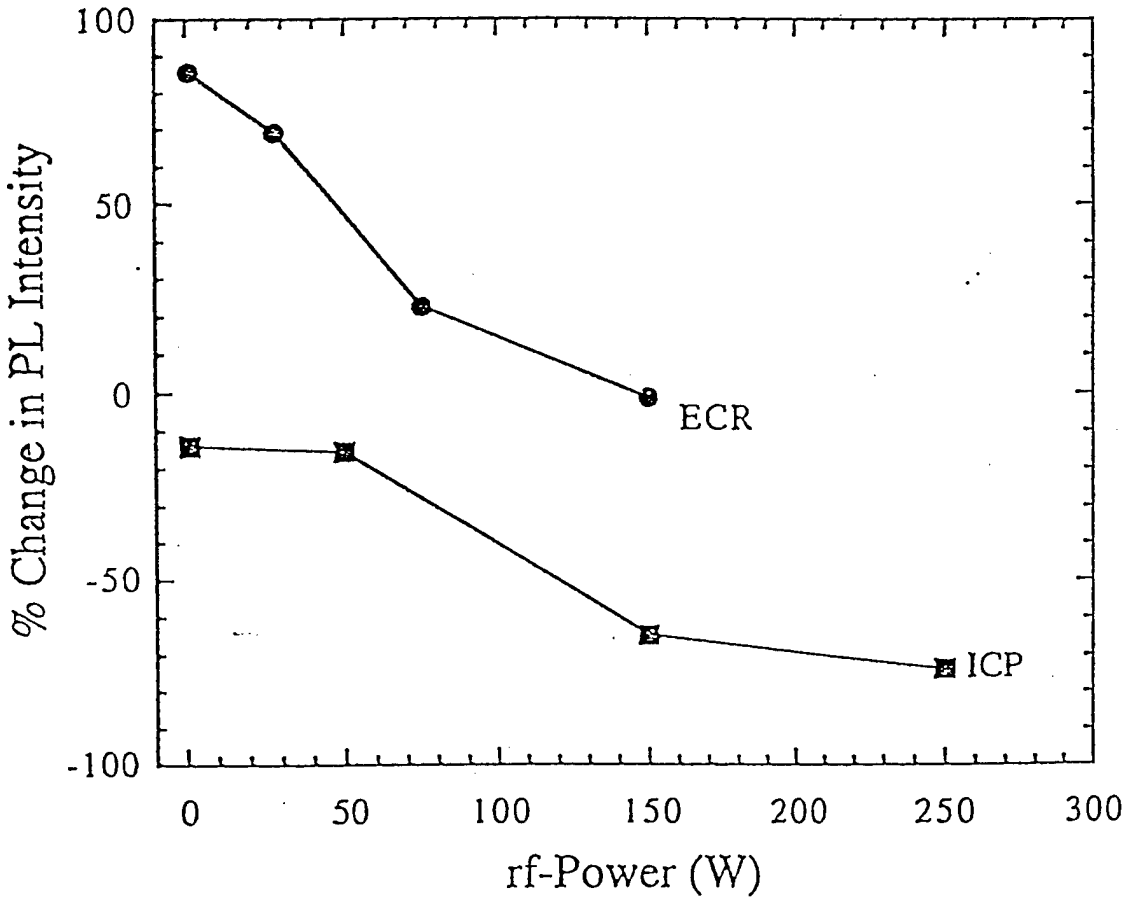

Figure 25 Percent change in the peak PL intensity as a function of rf power for ECR and ICP exposures.

The PL emission efficiency of other III-V bulk semiconductors (e.g. GaAs) has been shown to be strongly dependent on surface conditions, specifically the presence of a native oxide, the surface recombination velocity, as well as band bending at the surface.[14,15] Previous work on hydrogen plasma passivation in GaAs films with in-situ PL monitoring has demonstrated that both PL intensity enhancement as well as degradation can occur in different etching regimes. In particular, the reduction of surface As concentration in the initial stages of the etch can result in an increase in the PL efficiency whereas extended exposure to ion bombardment can create damage that reduces the PL efficiency.

While the exact nature of surface oxides and surface states in GaN are not well understood, our data show that the PL efficiency can be strongly affected by exposure to an Ar plasma and is highly sensitive to the exact plasma conditions. A common result for both plasma environments was the decrease in PL intensity with increasing rf-power which suggested that plasma-induced damage can occur in GaN films under moderate ion energies. Our initial data suggests that GaN surfaces are considerably more sensitive to process-inducted changes than is widely recognized. Brief low bias exposures to ECR discharges almost doubled the band-edge PL, suggesting that the native oxide has a strong effect on the surface recombination velocity. Work is in progress to more closely examine the changes in GaN surface conditions under various plasma conditions.

Post-etch anneals in Ar were performed on selected samples to investigate the effects of high temperature on the PL intensity. In Figure 26, we show the change in peak PL intensity as a function of anneal temperature for samples etched under 1 W, 150 W and 250 W rf-power in the ICP reactor. The post-etch condition, specifically the initial change in PL intensity due to the etch, is indicated at the "no anneal" condition. The data show that the effect of the anneal is strongly dependent on the initial (post-etch) sample conditions. In particular, the sample etched under very low power (1 W) degraded with increasing anneal temperature, whereas the sample etched under moderate power (250 W) showed an initial enhancement in the post-etch PL intensity, followed by degradation as the anneal temperature was increased beyond 400°C. These results suggested that relatively low temperature annealing may reduce the (non-radiative) damage induced under the 250 W etching conditions. In all cases, however, the effect of post-etch annealing in Ar for T >700°C resulted in a degradation of the PL intensity. At higher rf-powers we would expect a greater initial PL degradation because of the greater damage depth. The low temperature (≤400°C) annealing stage for the 250 W sample may result from the individual damage sites being closer together, as is seen in ion-implanted material, where annealing is actually easier in moderately damaged sample. However the key result is that overall, the etch damage is stable to >800°C, much higher than in other III-V materials.

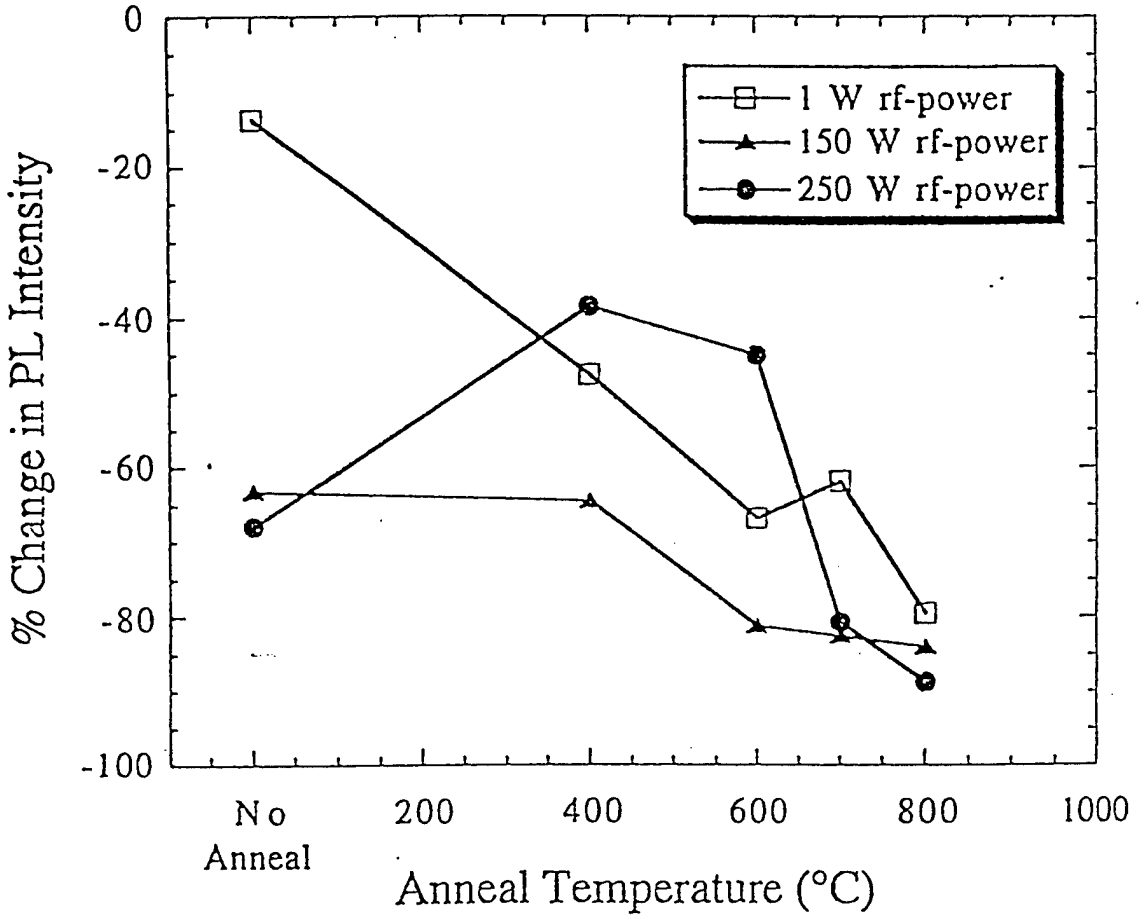

Figure 26 Percent change in the peak PL intensity as a function of post-etch anneal temperature for ICP etched samples, for different rf power conditions.

Similar post-etch annealing experiments were performed on selected samples etched in the ECR reactor, and the effect on PL intensity is shown in Figure 27. For all rf-power conditions, a degradation in the PL was seen after anneals at 400°C and 800°-C. The loss of PL intensity with anneal temperature was similar for all of the samples, in strong contrast to the ICP results. This result was not unexpected, due to the large differences in the PL intensities (post-etch) at the start of the anneal experiments. It is interesting to note that for the highest rf-power conditions, annealing at temperatures as high as 800°C resulted in a similar reduction of pre-etch PL intensity (75-90%) for both ICP and ECR etches, despite the large discrepancy in post-etch PL intensities.

In summary, peak PL intensity was strongly affected by exposure to an Ar ECR and ICP plasma, with both enhancement and degradation seen under various etch conditions, as is the case with GaAs. For both plasma environments the PL intensity decreased with increasing rf-power. Exposure to an ICP Ar plasma resulted in decreased PL intensity, whereas the PL intensity increased following exposure to the ECR. The effect of post-etch annealing in Ar varies, depending on initial film conditions. For all etch conditions examined in this work, annealing at temperatures above 400°C resulted in a reduction in the PL intensity. Possible degradation mechanisms may be due to defect migration to form stable non-radiative centers, loss of passivating hydrogen initially in the GaN, or the formation of a non-stoichiometric surface oxide. We are currently investigating all of these mechanisms using time-resolved PL and surface recombination velocity measurements. Although the nature of surface states and oxides in GaN is not entirely understood, our results suggest that surface conditions can significantly affect radiative recombination efficiency in GaN films. Further work is in progress to determine the nature and effect of plasma-induced surface passivation in the group-III nitride materials.

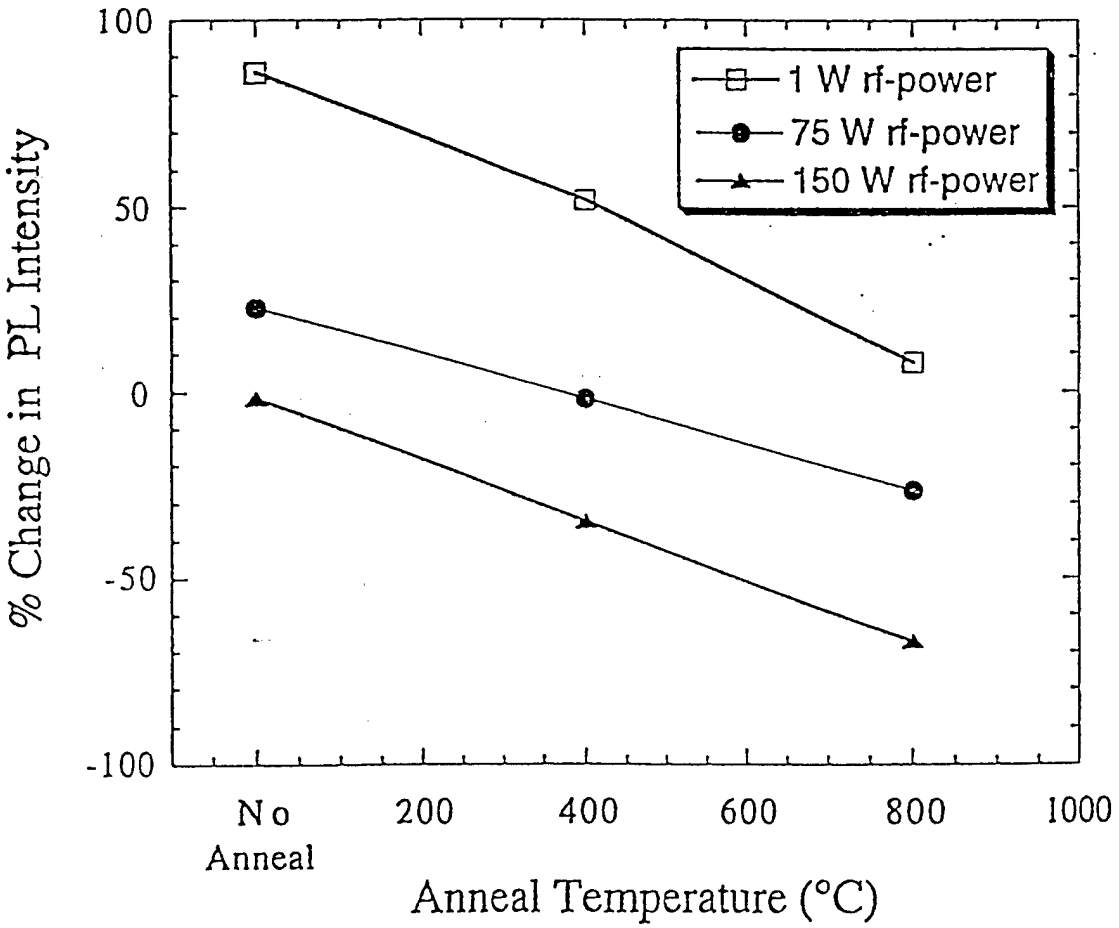

Figure 27 Percent change in the peak PL intensity as a function of post-etch anneal temperature for ECR etched samples, for different rf power conditions.

Photoelectrochemical Etching

Initial experiments were conducted on photoelectrochemical wet etching of GaN using Hg-lamp irradiation of samples immersed in KOH solutions. The etching was found to selectively reveal dislocations and grain boundaries when low etch-rate conditions were employed and to produce rough morphologies at high intensity illumination conditions. The morphologies became smoother on pre-annealed samples, indicating that near-surface defect density is a key factor.

Fabrication of Gratings

The GaN-InGaN laser diodes reported to date have been ridge waveguides in which the facets have been formed by dry etching, cleaving or polishing. These index-guided lasers have broad bandwidth and short coherence length, and are ideal for applications such as compact-disk players. Other applications such as communications require single-mode output, and the most common method for producing a resonant cavity for single frequency output is to form a periodic grating, either adjacent to the active regions through which current flows (distributed Bragg reflector laser). While the latter approach avoids the need for epitaxial regrowth on the grating, distributed feedback lasers are the most readily available form of semiconductor lasers.

To form sub-micron gratings (pitch ~3,000Å), samples were coated with 450Å thick imaging resist patterned by holographic exposure using the wavefront division method. The gratings were formed in both InGaN and GaN by room temperature etching with BCl_3/N_2 for short periods (30 sec – 2 min). Figure 28 shows AFM scans of gratings in GaN after removal of the remaining photoresist with acetone. The pattern transfer is uniform and complete, and the morphology between the gratings is similar to that of an unetched control sample.

Implantation and Thermal Processing

With regards to thermal processing, a new method of preserving the nitride surfaces during capless rapid thermal annealing was developed, as was the use of AlN encapsulants that can be selectively removed from GaN using KOH solutions.

A novel high temperature RTP system designed especially for processing of nitrides and based on molybdenum silicide aluminide alloy heating elements was investigated and has now been delivered for annealing implanted GaN at temperatures up to 1500°C. Activation efficiencies of > 90% were obtained for samples implanted with 5 x 10^{15} cm^{-2} Si^+ at 100 keV, and annealed at 1400°C with AlN caps. These caps were removed by selective KOH wet etching. Electron mobility was in the range 40-50 cm^2/V-sec for peak carrier concentration of ~ 5 x 10^{20} cm^{-3}. Without AlN capping the surface was found to deteriorate even at 1150 - 1200°C through preferential loss of N_2. Implantation of C^+ was found to compensate n-GaN, suggesting that carbon is an acceptor in this material, and explaining why activation efficiency often improves at higher doses because the effect of residual C backgrounds becomes relatively less important.

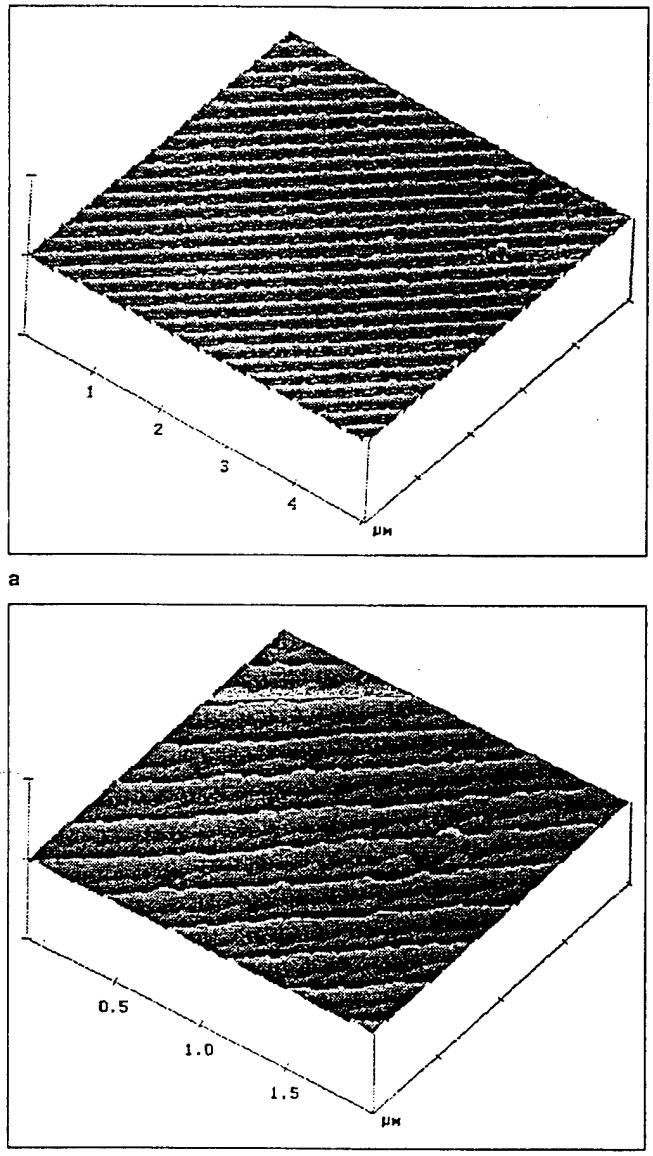

Figure 28. AFM scans of gratings formed in GaN. The resist has been removed.

Contacts

Refractory contacts based on W and WSix were investigated for use in high temperature devices. WSi_x Ohmic contacts on n^+-epi GaN (~10^{19} cm^{-3}) showed R_c values of ~10^{-4} Ω-cm^2, stable to 1000°C. Annealing up to 600°C had little effect on the WSi_x/GaN interface, but the B-W_2N phase formed between 700-800°C, concomitant with a strong reduction (factor of 2) in near-surface crystalline defects in the GaN. Spiking of the metallization down the threading and misfit dislocations was observed at 800°C, extending >500 nm in some cases. This can create junction shorting in laser structures by the same mechanism that limits laser lifetime in devices grown on unpatterned lattice-mismatched substrates. On implanted GaN, R_c values of < 10^{-6} Ω-cm^2 were obtained after 950°C annealing with values of ~10^{-5} Ω-cm^2 after 1050°C anneals. The lower R_c values compared to epi samples appear to be a result of the higher peak doping achieved, ~5 x 10^{20} cm^{-3}. SIMS profiles showed no measurable diffusion of the implanted Si, even at 1400°C, indicating that $D_{Si} \leq 10^{-13}$ cm^2/s at this temperature in GaN. We observed wide spreads in R_c values over a wafer surface, with the values on 950°C annealed material ranging from 10^{-7} to 10^{-4} Ω-cm^2. This is being increasingly reported for Ohmic contacts on GaN, but the obvious reasons (non-uniform surface contaminating residual oxides) have typically been ruled out. There appear to be highly non-uniform doping regions in the GaN, perhaps associated with the high defect density (~10^{10} cm^{-2}) in heteroepitaxial material, and this may contribute to the variations observed. We also believe that near-surface stoichiometry is variable in much of the GaN currently produced, due to the relative ease of preferential N_2 loss and the common use of H_2-containing growth (and cool down) ambients.

Finally the Ohmic contact behavior of WSi_x on abrupt and graded composition $In_XAl_{1-X}N$ layers has been studied as a function of growth temperature, InN mole fraction (X_{In} = 0 - 1), InN layer thickness and post WSi_x deposition annealing treatment. Contact layers were grown on (0001) sapphire in an Intevac Gas Source Gen II. The group III precursors, dimethylethylamine alane (DMEAA) and trimethylindium (TMI) were transported by a He carrier gas in order to avoid possible hydrogen passivation effects. An electron cyclotron resonance (ECR) plasma source (Wavemat MPDR 610) operated at 2.45 GHz and 200 W forward power was used to provide the nitrogen flux. N_2 flows of 20 sccm were used. Growth temperatures for In-containing layers ranged from 500°C to 575°C, while AlN layers were grown at 700°C. The growth sequence consisted of a nitridation step of 5 minutes at 700°C, followed by a low temperature (425°C) 500Å AlN nucleation layer and a 5000Å AlN buffer layer. Next, InAlN was grown to a thickness of 3000Å with a final InN cap layer of 500, 1000 or 2000Å. A 500Å graded region between the InAlN and the InN was used to avoid band discontinuities at the InN/InAlN interface. The film compositions were varied by altering the relative group III gas flow rates. Surface morphology was examined by scanning electron microscopy (SEM) and composition was analyzed with depth profile Auger electron spectroscopy (AES). Contact resistances were measured using the TLM method on WSi_x contacts fabricated by sputtering. Contact resistances were measured at room temperature on samples that were annealed in a rapid thermal annealer under flowing N_2 for five minutes at various temperatures.

As shown in Figure 29, the contact resistance of as-deposited contacts decreases substantially with increasing InN cap thickness up to 2000Å. While annealing of the 500Å structure produces a continual reduction in resistance over most of the range explored, annealing of the 2000Å structures does not appreciably change the electrical performance of the contact at temperatures up to 500°C. Interestingly, annealing at temperatures of 500° - 600°C produces roughly the same contact resistance for all of the InN thicknesses, suggesting that the contact resistance is being controlled by the formation of an interfacial layer at the contact/semiconductor interface or that the contact interface is being improved via intermixing at the interface.

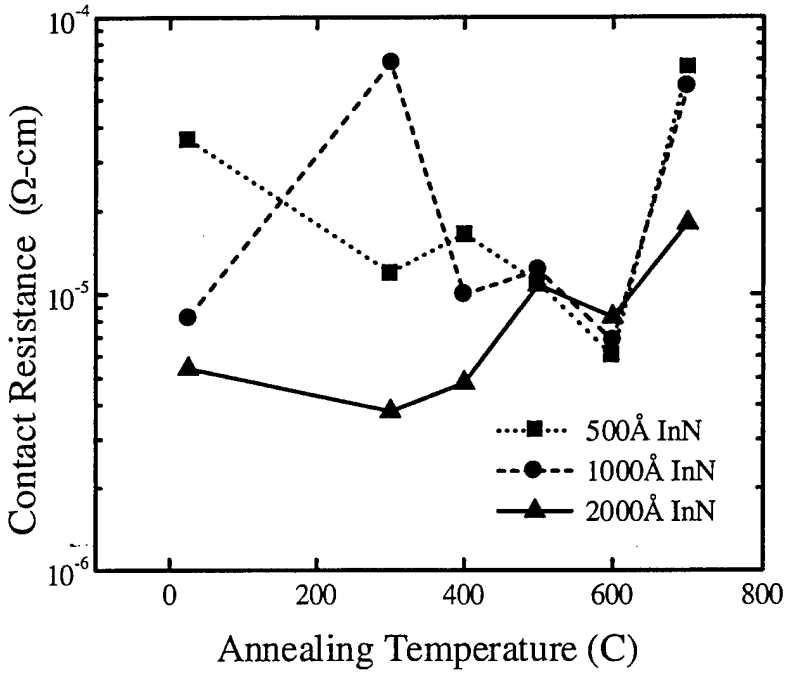

Figure 29. Contact resistance vs. annealing temperature for structures having 500, 1000 and 2000Å InN cap layers.

AES analysis of 500Å InN annealed contacts provides some insight into the observed electrical behavior. From the profiles shown in Figure 30, it would appear that the degradation in contact resistance after annealing at 700°C is most likely due to decomposition of the InN and subsequent diffusion of the In into the WSi_x. The contact structure in this case is now comprised of a WSi_x/AlInN junction which would be expected to exhibit a poorer contact. As also seen in Figure 30, annealing at 600°C appears to induce some intermixing of the InN and the WSi_x which could explain the improved contact resistance relative to that observed in the as-deposited sample.

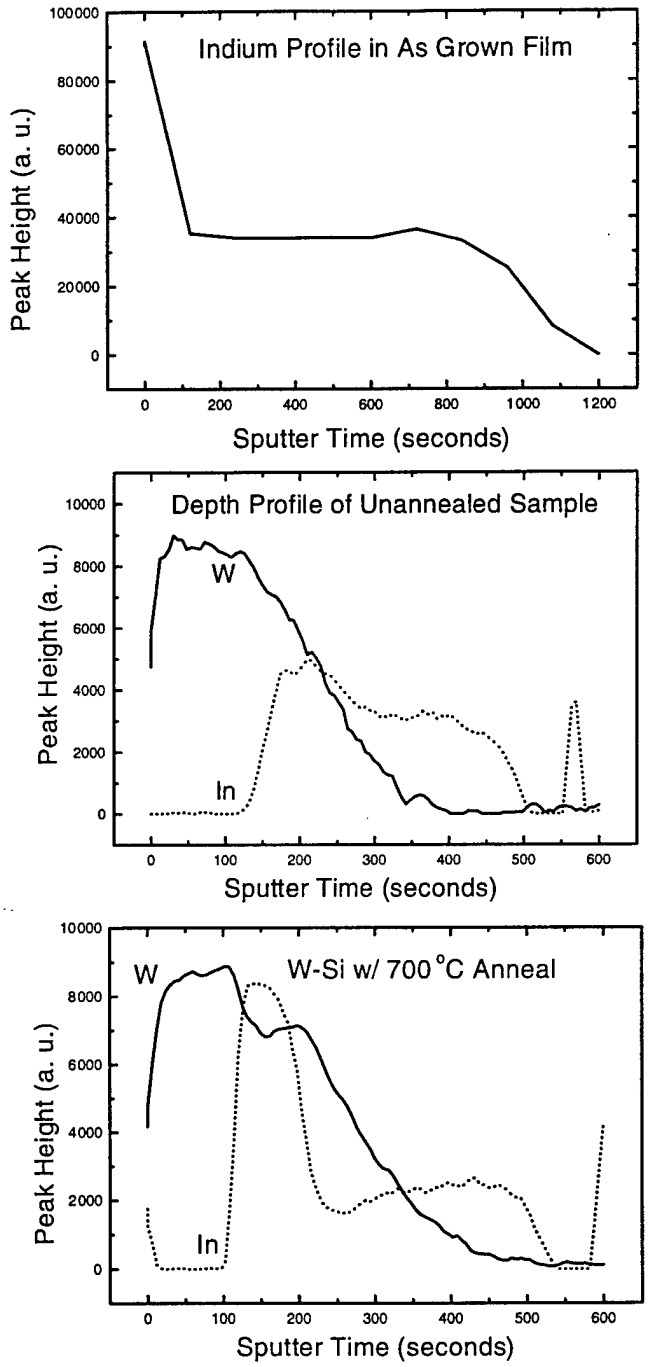

Figure 30. Depth profile AES curves of as grown sample (top), unannealed contact structure (middle) and contact structure annealed at 700 °C.

Unfortunately, while annealing at temperatures less than 700°C improves the electrical quality, it can have an adverse effect on the adhesion, which worsens as the InN thickness is increased. For 2000Å structures, even 400°C anneals cause some bubbling of the contact metal, as shown in Figure 31. This behavior is similar to that observed for InAs-based contacts on GaAs, where increasing thickness has been shown to reduce the maximum allowable processing temperature. This may be due at least in part to the difference in lattice constant and thermal properties of InN relative to the underlying InAlN, and to the strong temperature dependence of the InN equilibrium nitrogen vapor pressure. The best compromise considering both performance and stability appears to be the use of 1000Å layers. This contact structure provided good electrical behavior both with and without annealing while good adhesion was maintained even at annealing temperatures up to 700°C. Though resistance measurements as a function of testing temperature are needed to further quantify the thermal stability of these layers, these preliminary results suggest that these structures may be adequate for use in high temperature electronic applications.

Material Purity

The purity of various group III and dopant precursors used in synthesis of III-Nitrides has been evaluated. It has been determined that many of the commonly used compounds contain ether which is most likely the cause of much of the oxygen and carbon contamination often seen in these materials. TMIn and TEG are particularly problematic. Dopant sources not synthesized with ether, such as DMEAA and Cp_2Mg, do not appear to suffer from this problem. A collaboration with EpiChem was initiated to eliminate this contamination. As a result, we evaluated alternatives to conventional TMI such as solution TMI, which are expected to reduce the amount of ether transmitted to the growth surface. We have found that InN grown with TMI is highly defective single crystal, as shown in the XTEM and SADP data shown in Figure 32. The dislocation densities are comparable to those reported for GaN and AlN grown on sapphire. Unfortunately, all of the films grown with TMI exhibit n-type conduction with carrier concentrations in the 10^{20} - 10^{21} cm^{-3} range (Table II). The mobilities obtained in these films compare favorably with material grown by other techniques, as shown in Figure 33. SIMS analysis of these films shows both carbon and oxygen to be present at high concentrations. The carbon is most likely arising from the methyl radicals released by pyrolysis of the TMI, while the oxygen is probably introduced by residual ether left over from the TMI synthesis. It should be noted that GaN grown in the same chamber under similar N_2 plasma conditions using solid Ga contains impurities at levels one to two orders of magnitude lower than observed for TMI derived InN.

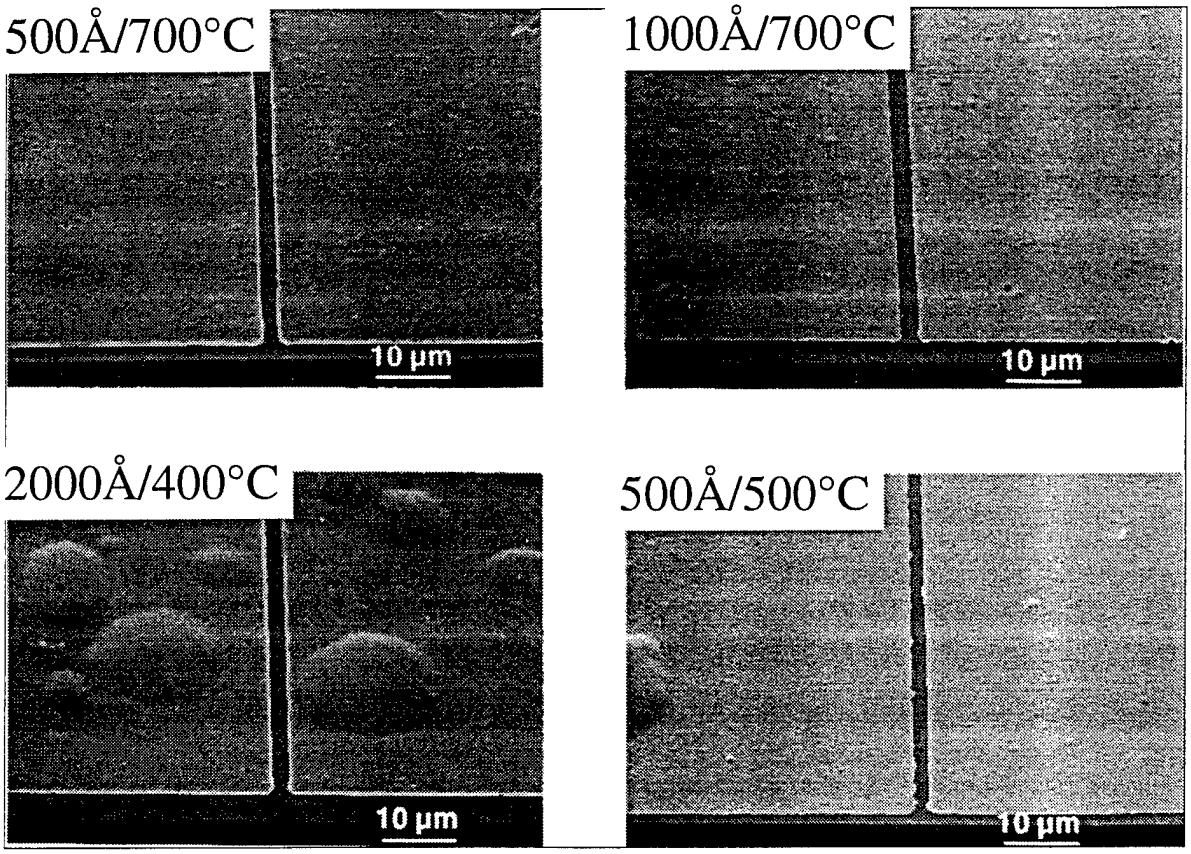

Figure 31. Scanning electron micrographs of contact structures showing effect of annealing temperature and InN cap layer thickness on surface morphology.

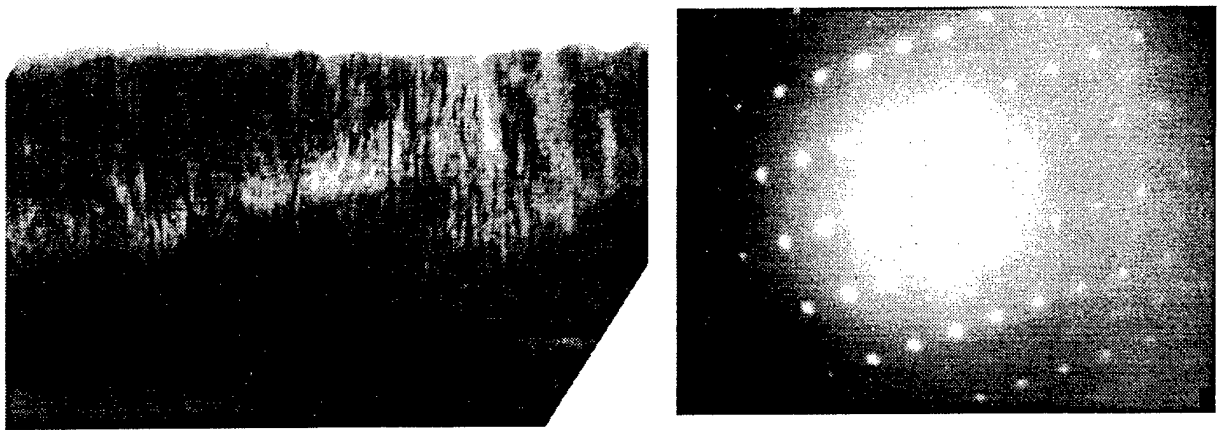

Figure 32. *XTEM micrograph, at left, and selected area diffraction pattern, at right, of InN grown from TMI on sapphire. The absence of streaks in the SADP pattern is indicative of single crystal material.*

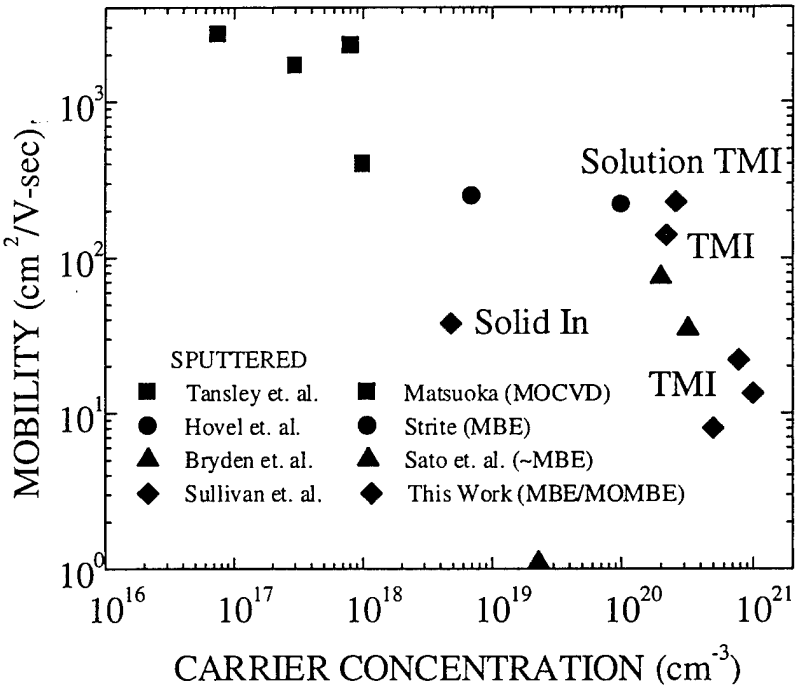

Figure 33: *Mobility vs. electron concentration for InN grown using various techniques and sources. Data from [16-24].*

Not surprisingly, InN grown from solution TMI also exhibits a high as-grown electron concentration, as shown in TABLE II. As for TMI, the mobilities are comparable to those reported in the literature (Figure 33). The carbon background obtained with solution TMI is similar to that derived from standard TMI at 1.9×10^{20} cm^{-3}. By contrast to the TMI-derived material, the oxygen background using solution TMI is significantly lower at 8×10^{18} cm^{-3}. This lends further credence to the identification of ether as the source of the oxygen in the TMI-derived material since the dimethyldodecylamine (DMDA) used to liquefy the solution TMI is believed to displace the ether. Further, the similarity between the electron and carbon concentrations suggests that in this material the electrical activity may be dominated by impurities rather than nitrogen vacancies. Based upon bond strength considerations, carbon is in fact expected to behave as a donor.[18]

TABLE II: *Impurity contamination, as determined by SIMS, and electron concentration, as determined by Hall, for InN grown using various sources.*

SOURCE	[C] (cm^{-3})	[O] (cm^{-3})	Electron Concentration (cm^{-3})
TMI	10^{20} - 10^{21}	10^{20}-10^{21}	10^{20}-10^{21}
Solution TMI	1.9×10^{20}	8×10^{18}	2×10^{20}
Solid In	-	-	$\leq 8 \times 10^{18}$

As expected, the as-grown electron concentration of the InN obtained using solid In is significantly reduced relative to that obtained from the alkyl sources (TABLE II). While this is most likely due to a reduction in the impurity background, this cannot yet be stated conclusively since SIMS analysis has not yet been successfully obtained. This analysis is complicated by the very rough morphology of the solid In derived layers, as shown in Figure 34. This extreme roughness is believed to be due to the poor surface mobility of the elemental In. While somewhat better films have been obtained on GaAs, morphologies in films grown on sapphire have been extremely rough, independent of nitrogen source (ECR vs. RF) and growth rate.

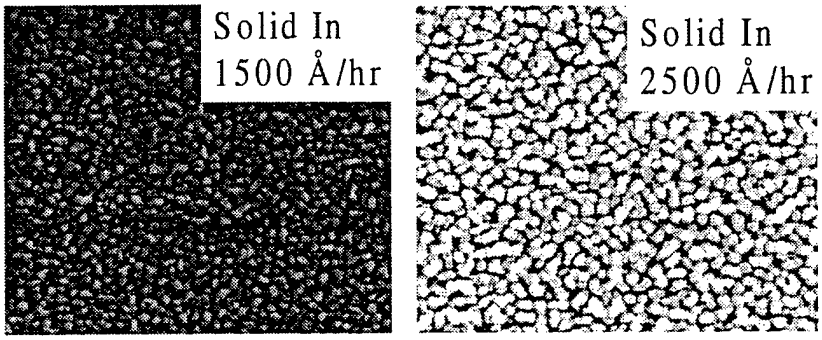

Figure 34. *SEM micrographs of InN grown on sapphire using a solid In source. The highly columnar surface most likely results from poor surface mobility and is independent of growth rate. (Magnification = 10kX.)*

SUMMARY OF ACCOMPLISHMENTS

- Low damage dry etching processes for all of the nitride materials were developed.
- The first gratings for DFB laser use were formed in GaN using holographic lithography and dry etching.
- A high temperature annealing process for GaN was developed.
- Thermal stability limits were established for W, WSi and Ti/Al ohmic contacts on InGaN alloys across the entire In composition range.
- Impurity sources in the gaseous In precursor TMI were identified.

PUBLICATIONS RESULTING FROM THIS PROGRAM

1. "Wet Chemical Etching of AlN and InAlN in KOH Solutions," C.B. Vartuli, S.J. Pearton, J.W. Lee, C.R. Abernathy, J.D. MacKenzie, J.C. Zolper, R.J. Shul and F. Ren, Journal of Electrochemical Society 143, 3681-3685 (1996).

2. "Thermal Stability of W, WSix and Ti/Al ohmic contacts to InGaN, InN and InAlN," C. B. Vartuli, S. J. Pearton, C. R. Abernathy, J. D. MacKenzie, R. J. Shul, J. C. Zolper, M. L. Lovejoy, A. G. Baca and M. Hagerott-Crawford, J. Vac. Sci. and Technol. **14**, 3520 (1996).

3. "Comparison of Ohmic Metallization Schemes for InGaAlN," F. Ren, C.B. Vartuli, S.J. Pearton, C.R. Abernathy, S.M. Donovan, J.D. MacKenzie, R.J. Shul, J.C. Zolper, M.L. Lovejoy, A.G. Baca, M.H. Crawford and K.A. Jones, Journal of Vacuum Science Technology A 15,802-805 (1997).

4. "Rapid Thermal Processing of III-Nitrides," J. Hong, J.W. Lee, C.B. Vartuli, C.R. Abernathy, J.D MacKenzie, S.M. Donovan, S.J. Pearton and J.C. Zolper, Journal of Vacuum Science Technology A 15, 797-800 (1997).

5. "High Temperature Annealing of GaN, InN and AlN and Related Alloys," J. Hong, J. Lee, C. Vartuli, J. MacKenzie, S. Donovan, C.R. Abernathy, R. Crockett, S.J. Pearton, J.C. Zolper and F. Ren, Solid State Electronics 41, 681-683 (1997).

6. "Formation of Dry Etch Gratings in GaN and InGaN," J.W. Lee, J. Hong, J. MacKenzie, C.R. Abernathy, S.J. Pearton, F. Ren and D. Sirortino, Journal of Electronic Materials 26, 290-293 (1997).

7. "Wet Chemical Etching of AlN and InAlN in KOH Solutions," C.B. Vartuli, S.J. Pearton, J.W. Lee, C.R. Abernathy, J.D. MacKenzie, J.C. Zolper, R.J. Shul and F. Ren, Journal of Electrochemical Society 143, 3681-3685 (1996).

8. "Comparison of GaN, InN and AlN Powders for Susceptor-based Rapid Thermal Annealing of Group III-Nitride Materials," J. Hong, J.W. Lee, J.D. MacKenzie,

S.M. Donovan, C.R. Abernathy, S.J. Pearton and J.C. Zolper, Semicond. Sci. Technol. 12, 1310 (1997).

9. "Conduction Mechanisms in W and WSi_x Ohmic Contacts to InGaN and InN," C. Vartuli, S.J. Pearton, C.R. Abernathy, J. MacKenzie, M. Lovejoy, R. Shul, J. Zolper, A.G. Baca, M. Crawford, A. Jones and F. Ren, Solid State Electronics 41, 531-534 (1997).

10. "Effect of BCl_3 Dry Etching on InAlN Surface Properties," F. Ren, J. Lothian, Y.K. Chen, J.D. MacKenzie, S.M. Donovan, C.B. Vartuli, C.R. Abernathy, J.L. Lee and S.J. Pearton, Journal of Electrochemical Society 143, l217-l219 (1996).

11. "Selective Dry Etching of III-V Nitrides in Cl_2/Ar, CH_4/H_2/Ar, ICl/Ar and IBr/Ar," C.B. Vartuli, S.J. Pearton, J.D. MacKenzie, C.R. Abernathy and R.J. Shul, Journal of Electrochemical Society 143, L246-L247 (1996).

12. "High Density Etching of Group III Nitride Ternary Films," R.J. Shul, A.J. Howard, S.J. Pearton, C.R. Abernathy and C.B. Vartuli, Journal of Electrochemical Society 143, 3285-3290 (1996).

13. "Substrate Effects on Growth of InN," S. Donovan, J. MacKenzie, C.R. Abernathy, P. Holloway, F. Ren, J. Zavada and B. Choi, Fall Materials Research Society Meeting Proceedings Vol. 468, 161-166 (1997).

14. "ICP Dry Etching of III-Nitrides," C. Vartuli, J. Lee, J. MacKenzie, C.R. Abernathy, S.J. Pearton, R.J. Shul, A. Katz, A.Y. Polyakov and M. Shin, 1997 Fall Materials Research Society Meeting Proceedings Vol. 468, 393-399 (1997).

15. "Current Transport in W and WSi_x Ohmic Contacts to InGaN and InN," C. Vartuli, S.J. Pearton, C.R. Abernathy, J. Mackenzie, M. Lovejoy, R. Shul, J. Zolper, A. Baca, K. Jones and F. Ren, 1997 Spring MRS Meeting, San Francisco, 1997 Fall Materials Research Society Meeting Proceedings Vol. 468, 413-419 (1997).

16. "Development of GaN and InGaN Gratings by Dry Etching," J. Lee, J. Hong, J. MacKenzie, C.R. Abernathy, S.J. Pearton, F. Ren and P. Sciortino, 1997 Fall Materials Research Society Meeting Proceedings Vol. 468, 379-384 (1997).

17. "Chemical Etching of AlN and InAlN in KOH Solutions," C.B. Vartuli, J.W. Lee, J.D. MacKenzie, S.J. Pearton, C.R. Abernathy, J.C. Zolper, R.J. Shul and F. Ren, 1996 Fall Materials Research Society Meeting Proceedings Vol. 462 264-269 (1997).

18. "Optimization of InN Growth by MOMBE for Improved III-N Contact Performance," S.M. Donovan, J.D. MacKenzie, C.R. Abernathy, C.B. Vartuli, S.J. Pearton, F. Ren, M.W. Cole and K. Jones, 1996 Fall Materials Research Society Meeting Proceedings Vol. 462, 511-513 (1996).

19. "Plasma Etching of III-Nitrides in ICl/Ar and IBr/Ar Plasmas," C.B. Vartuli, J.W. Lee, J.D. MacKenzie, S.J. Pearton, C.R. Abernathy and R.J. Shul, 1996 Fall Materials Research Society Meeting Proceedings Vol. 462, 277-281 (1996).

20. "W_4WSi_x and Ti/Al Low Resistance Ohmic Contacts to InAlN and InN," C.B. Vartuli, S.J. Pearton, C.R. Abernathy, J.D. MacKenzie, R. Shul and J.C. Zolper, 1996 Materials Research Society Meeting Proceedings Vol. 422,97-101 (1996).

21. "Thermal Stability of Ohmic Contacts to InN," S. M. Donovan, J. D. MacKenzie, C. R. Abernathy, S. J. Pearton, F. Ren, K. Jones and M. Cole, Solid State Electron. **42** 1831 (1998).

22. "The Role of the In Source in InN Growth from Molecular Beams," Mat. Res. Soc. Symp. Proc. Vol. **512**, 525 (1998).

23. "Cl_2-based Dry Etching of the AlGaInN System in Inductively Coupled Plasmas," H. Cho, C. B. Vartuli, C. R. Abernathy, S. M. Donovan, S. J. Pearton, R. J. Shul and J. Han, Mat. Res. Soc. Symp. Proc. Vol. **483**, 327 (1998).

REFERENCES

1. C.B. Vartuli, S.J. Pearton, J.W. Lee, C.R. Abernathy, J.D. MacKenzie, J.C. Zolper, R.J. Shul and F. Ren, J. Electrochem. Soc. **143**, 3681 (1996).

2. C.R. Abernathy, Mat. Sci. Eng. Rep. **14**, 203 (1995).

3. J.R. Mileham, S.J. Pearton, C.R. Abernathy, J.D. MacKenzie, R.J. Shul and S.P. Kilcogne, Appl. Phys. Lett. **67**, 1119 (1995).

4. CRC Handbook of Chemistry and Physics (Chemical Rubber, Boca Raton, FL, 1990).

5. W.A. Harrison, Electronic Structures and Properties of Solids (Freeman, San Francisco, 1980).

6. S.J. Pearton, C.R. Abernathy, F. Ren and J.R. Lothian, J. Appl. Phys. **76**, 1210 (1994).

7. R.J. Shul, C.T. Sullivan, M.B. Snipes, G.B. McClellan, M. Hatich, C.T. Fuller, C. Constantine, J.W. Lee and S.J. Pearton, Solid State Electron. 38, 2047 (1997).

8. S.W. Pang, J. Electrochem. Soc. 133, 784 (1986).

9. C. Constantine, D. Johnson, S.J. Pearton, U.K. Chakrabarti, A.B. Emerson, W.S. Hobson and A.P. Kinsella, J. Vac. Sci. Technol. B8, 596 (1990).

10. S.J. Pearton, J.W. Lee, J.D. MacKenzie, C.R. Abernathy and R.J. Shul, Appl. Phys. Lett. 67, 2329 (1995).

11. C. Yuan, T. Salagaj, A. Gurary, P. Zawadzki, C.S. Chern, W. Kroll, R.A. Stall, Y. Li, M. Schurman, C.-Y. Hwang, W.E. Mayo, Y. Lu, S.J. Pearton, S. Krishnankutty and R.M. Kolbas, J. Electrochem. Soc. 142, L163 (1995).

12. W. Shan, T.J. Schmidt, X.H. Yang, J. Hwang, J.J. Song and B. Goldenberg, Appl. Phys. Lett. 66, 985 (1995).

13. G.D. Chen, M. Smith, J.Y. Lin, H.X. Jiang, M. Asif Kahn and C.J. Sun, Appl. Phys. Lett. 67, 1653 (1995).

14. R.A. Gottscho, B.L. Preppernau, S.J. Pearton, A.B. Emerson and K.P. Giapis, J. Appl. Phys. 68, 440 (1990).

15. E.S. Aydil and R.A. Gottscho, Mat. Sci. For. 148/149, 159 (1994).

16. H. J. Hovel and J. J. Cuomo, Appl. Phys. Lett. **20** 71 (1972).

17. T. L. Tansley and R. J. Egan, Physica B **185** 190 (1993)..

18. T. L. Tansley and C. P. Foley, Elec. Lett. **20** 1066 (1984).

19. W. A. Bryden, S. A. Ecelberger, J. S. Morgan, T. O. Poehler and T. J. Kistenmacher, *Mater. Res. Soc. Symp. Proc.* **242** 409 (1992).

20. B. T. Sullivan, R. R. Parsons, K. L. Westra and M. J. Brett, J. Appl. Phys. **64** 414 (1988).

21. T. Matsuoka, J. Cryst. Growth, **124**, 433 (1992).

22. S. Strite and H. Morkoc, J. Vac. Sci. and Technol. **B10** 1237 (1992), and references therein.

23. S. Strite, D. Chandrasekhar, D. J. Smith, J. Sariel, H. Chen, N. teraguchi, H. Morkoc, J. Crystal Growth, **127**, 204 (1993).

24. Y. Sato and S. Sato, Mat. Sci. and Eng. B **35** 171 (1995), and references therein.

25. W. Schoenfeld, M. J. Antonell and C. R. Abernathy, J. Crystal Growth, **188**, 50 (1998).